REACTOR CORE ISOLATION COOLING PUMP PERFORMANCE IN MULTIPHASE CONDITIONS

A Thesis

by

ZACHARY R. STRATER

Submitted to the Office of Graduate and Professional Studies of
Texas A&M University
in partial fulfillment of the requirements for the degree of

MASTER OF SCIENCE

Chair of Committee,	Karen Vierow Kirkland
Committee Members,	Gerald Morrison
	Mark Kimber
Head of Department,	Yassin Hassan

December 2017

Major Subject: Nuclear Engineering

ABSTRACT

The Reactor Core Isolation Cooling (RCIC) system is found in certain boiling water reactor power plants. The RCIC system is meant to provide coolant to the reactor pressure vessel (RPV) in certain cases when the vessel is isolated from the main steam turbines and condensers. In 2011, the Great East Tohoku earthquake in Japan caused the operation of three reactors at the Fukushima Daiichi nuclear site to be interrupted. The seismic activity initiated the shutdown of the three reactors and the RCIC system came online in the two reactors equipped with a RCIC system.

The RPV must have decay heat removal after shutdown. In the Fukushima Daiichi nuclear accident the RCIC system, it is believed, removed this decay heat from units 2 and 3 for 70 and 20 hours respectively. This greatly exceeds the expected RCIC run time of 4-8 hours, which is why the RCIC system has drawn great amounts of attention since the accidents. Experimental demonstration of this extended operation of the RCIC system shows that the system could be more capable of providing cooling than previously thought. As this performance in practice is far greater than the anticipated operation duration, the RCIC system merits increased study into its performance, specifically, in beyond design accidents and station blackout conditions.

A Computational Multiphase Fluid Dynamics (CMFD) simulation was developed herein for implementation in STAR-CCM+. This simulation studied

the RCIC pump performance and degradation due to changes in turbine performance and heat up of the Suppression Pool. As the RCIC pump and turbine are physically on the same shaft, the turbine's performance has direct implications on the performance of the pump. One of the pump suction sources is the Suppression Pool, so a heat up of the Suppression pool could introduce two-phase flow at the pump inlet. A centrifugal pump similar to those used in RCIC Systems was created in the CMFD model to explore the pump performance as it is affected by Gas Void Fraction, and impeller rotational speed.

The goal of this thesis is to develop, implement, and apply detailed mathematical models of the RCIC system pump so its performance in beyond design accident and station blackout conditions can be better understood.

DEDICATION

For my family. Thank you.

ACKNOWLEDGEMENTS

I would like to express my abundant appreciation to Dr. Karen Kirkland for her guidance and support. Her knowledge, intelligence and patience helped solve many problems throughout my research. I would also like to thank my committee members: Dr. Mark Kimber and Dr. Gerald Morrison for their support. Kyle Ross and Brad Beeny and the rest of the staff at Sandia for answering any questions I had. Corey Clifford, Juan Reyes and Edward Kraft for their unconditional help on my research. I would like to thank Lauren Hook for her support in my education. Finally, thanks to my Mother and father for their encouragement throughout my research.

CONTRIBUTORS AND FUNDING SOURCES

This work was supervised by a thesis committee consisting of Professor Kirkland and Professor Kimber of the Department of Nuclear Engineering and Professor Morrison of the Department of Mechanical Engineering.

All work for the thesis was completed independently by the student.

This work was made possible in part by the Department of Energy Nuclear Engineering University Program under Grant Number #DE-NE008312.

Its contents are solely the responsibility of the author and do not necessarily represent the official views of the Nuclear Engineering University Program.

NOMENCLATURE

ACRONYMS

AC	Alternating Current
BWR	Boiling Walter Reactor
CFD	Computational Fluid Dynamics
CMFD	Computational Multiphase Fluid
CST	Dynamics Condensate Storage Tank
DC	Direct Current
RCIC	Reactor Core-Isolation Cooling
RPM	Revolutions per Minute
RPV	Reactor Pressure Vessel
TDR	Turbulent Dissipation Rate
TKE	Turbulent Kinetic Energy
SBO	Station Blackout

UNITS

Kg/s	Kilograms per second
GPM	Gallons per Minute
Pa	Pascals
S	seconds

TABLE OF CONTENTS

LIST OF FIGURES

Page

LIST OF TABLES

Page

1 INTRODUCTION

In the spring of 2011, a massive earthquake occurred in the ocean just east of Japan. The large earthquake induced large tsunamis that impacted the operation of the Fukushima Daiichi nuclear power plant. Off-site power was lost to all six units at the Fukushima Daiichi site due to the seismic activity in the region. The tsunami that followed the earthquake caused a disruption to the DC power to units 1, 2 and 4. The seismic activity and resulting tsunamis caused all six Fukushima Daiichi units to enter into Station Blackout (SBO) conditions for an extended time period [1].

The reactors at Fukushima Daiichi units 2 and 3 are of a General Electric BWR 4 design with a Mark I containment. Fukushima Daiichi units 2 and 3 utilize the Reactor Core Isolation Cooling (RCIC) system for core heat removal during isolation from the main steam turbines [2]. The RCIC system provides water flow to the Reactor Pressure Vessel (RPV) to remove decay heat. In conditions such as those of the Fukushima Accident, the RCIC system relies on DC power from backup batteries. These batteries are expected to be depleted within four to eight hours, which results in loss of power to the RCIC turbine governor valve. By design, loss of all electrical power to the RCIC system results in the turbine governor valve failing in the fully open position. With full steam flow entering the turbine, the turbine should speed up rapidly, causing the

turbine to trip on over speed shortly after. Reactor core cooling is thereby terminated unless another heat removal system can be brought online.

Fukushima Daiichi Units 2 and 3 were both able to greatly out perform their rated cooling time of four to eight hours [3]. Unit 2 was able to operate for approximately 70 hours. In Unit 2, both AC power and DC power were interrupted due to the flooding caused by the tsunami. The leading hypothesis as to the mechanism for long-term operation is that the turbine governor valve froze in a favorable position which avoided an overspeed trip [4].

The present research is an investigation of the RCIC pump operation under long-term SBO conditions. A thorough understanding of the cause of this extended operation would be useful in better understanding of the events occurring in the RCIC system of the Fukushima Daiichi accident. This research would be useful in predicting future operation of the RCIC system in SBO conditions.

Appropriately in-depth overviews of the RCIC system and STAR-CCM+ are given in thesis sections 2 and 4. Section 2 includes background information on the Fukushima accident, a detailed description of the RCIC system, an overview of the turbo-pump assembly, and a discussion of some RCIC operational characteristics. Section 3 includes a high level discussion to centrifugal pumps and describes the process of imparting energy to the fluid. Section 4 includes an introduction to STAR-CCM+ and sufficiently descriptive

summaries of its code mechanics, solution workflow, and selected code features/concepts of importance to pump modeling.

Sections 5 and 6 provide greater detail of the simulation setup and uncertainty of the model. Section 5 outlines the ideologies including equations, and formulations useful for CMFD analyses. The ideologies discussed in section 5 are used to create the model that simulates accident conditions in the RCIC pump. Section 6 discusses the uncertainty of the model including a grid independence study.

Sections 7 and 8 discuss the results obtained from the implementation of models described in section 5 and final conclusions. The results from the model implementation are discussed in Section 7. Section 8 brings final thoughts of the research and possible future work that can be done in the topic.

2 BACKGROUND

Following the Great East Japan Earthquake, each nuclear power unit of Fukushima Daiichi was subject to a unique set of operating conditions. Both units 2 and 3 operate with BWR 4 designs and Mark I containments. As previously discussed, units 2 and 3 utilized the RCIC system, which allow operation for up to eight hours. The unit 3 RCIC had battery power available and operated for approximately 20 hours before the turbine tripped, due to High Pressure Core Injection activation. Unit 2, with battery power interrupted, operated for approximately 70 hours. For this reason, the Unit 2 RCIC system is the unit of study for this project.

Several factors are hypothesized to have affected the extended RCIC operation in Unit 2. The system could have failed because of multiple reasons: moisture carryover into the turbine, pump cavitation, and erratic governor control. All of these conditions were likely present and could have all caused failure of the RCIC system, however none terminated the system until 70 hours.

The RCIC system operates by taking steam produced by the Reactor Pressure Vessel (RPV) to spin a turbine. This turbine is directly coupled to a pump, via a shaft through the center of the turbine and pump. The coupling of a terry turbine and centrifugal pump can be seen in figure 1.

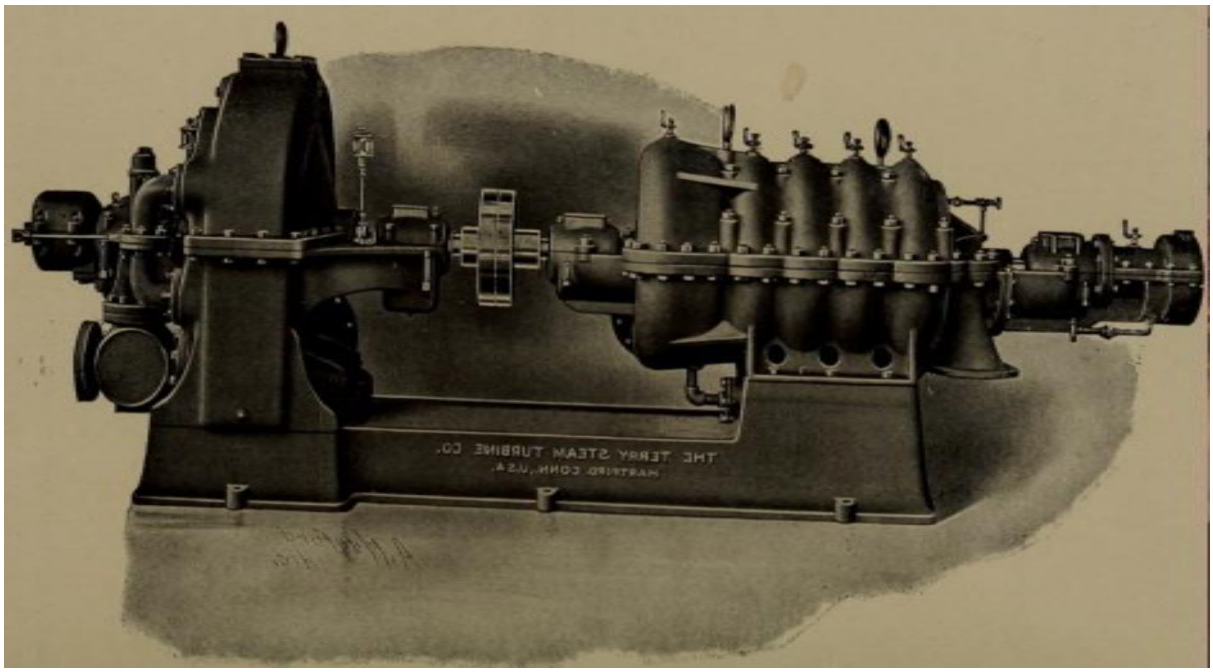

Figure 1: Terry turbine coupled to centrifugal pump. [5]

The regulation of the turbine speed is dependent on a DC power supply. The RCIC pump takes suction from one of two sources: The Condensate Storage Tank (CST) or the suppression chamber. Pump discharge is directed in two directions: a majority going to the RPV, and a small portion to the turbine auxiliaries. For ease, the discharge to the turbine auxiliaries is ignored in schematics. Figure 1 is a representative diagram of the RCIC system.

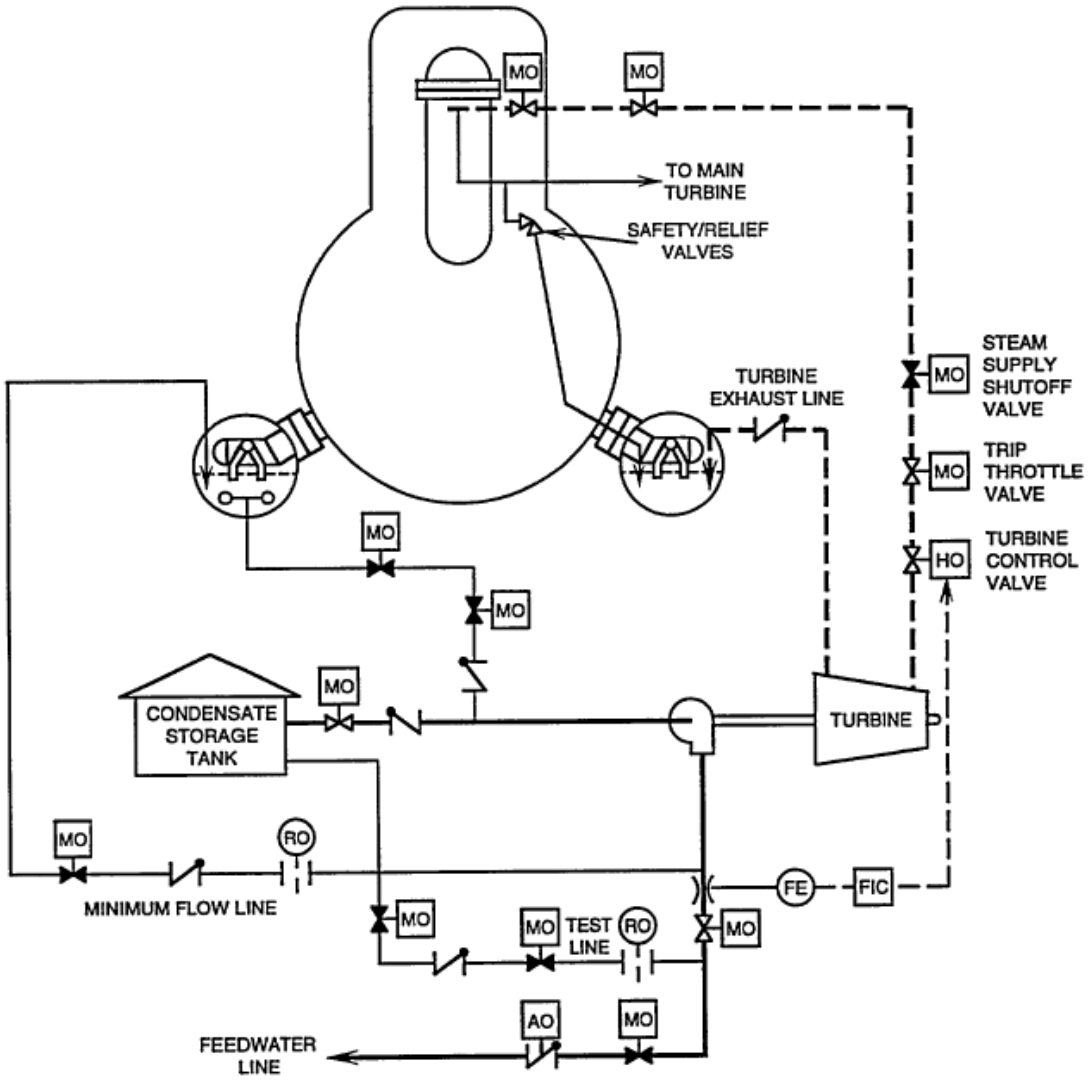

Figure 2: Diagram of RCIC system for BWR/4 with Mark I Containment [2].

During the Fukushima Daiichi accident, injection rates from the RCIC pump into the core are unknown. Later, Modular Accident Analysis Program (MAAP) showed that the RCIC pump was operating at 1/3 efficiency [6]. This was assumed to be due to the decreased efficiency of the RCIC turbine.

When the power was lost all instrumentation in the RPV lost power as well. This allowed the RPV to have an increased water capacity. The increased water capacity translates into water spillover from the RPV into the main steam lines. The moisture in the steam line would then compound by carrying over into the RCIC turbine. Water ingestion in the RCIC turbine should decrease the performance of the turbine and directly result in the reduced efficiency of the pump.

2.1 RCIC System Speed Control

The RCIC system responds to inputs from many sources, including but not limited to: Trip and Throttle Valve (TTV), steam from reactor, and DC power. The TTV is a valve that responds in case of an over speed trip of the turbine. The turbine takes steam through the TTV and shuts when the turbine begins to rotate at a speed greater than safely operable. There is also instrumentation that detects the inlet flow rate in relation to the desired inlet flow rate. The governor system operates with this instrumentation to maintain the desired inlet flow rate by controlling the oil pressure. This results in an increase or decrease of turbine rotation speed. Since the turbine is coupled to the pump impellers this results in an increase or decrease of pump impeller speed. This instrumentation, however, required DC power which was lost in the Fukushima Accident. In these cases, the Governor valve will then move to a fully opened position and there is no longer an over speed trip.

2.2 RCIC System Pump Characteristics

The RCIC system is a widely used system in the nuclear industry. There are many different RCIC pumps that vary from plant to plant. There are, however, similarities between all RCIC pumps. The RCIC pump is a turbine driven, horizontal, multi-stage, centrifugal pump. a representative RCIC pump is designed to deliver a minimum of 425 Gallons per minute (GPM), meaning most are rated to deliver around 600 GPM. The minimum flow rate into the reactor core is 400 GPM. This flow rate is the required flow to remove the residual heat form the Reactor core for 15 minutes. The remaining 25 GPM required is delivered to the turbine auxiliaries, helping to prevent the turbine from overheating. The minimum NPSH requirement (varies plant to plant) is obtained by placing the pump in a lower axial position than its suction sources. In Figure 3, a pump schematic is shown for the RCIC pump.

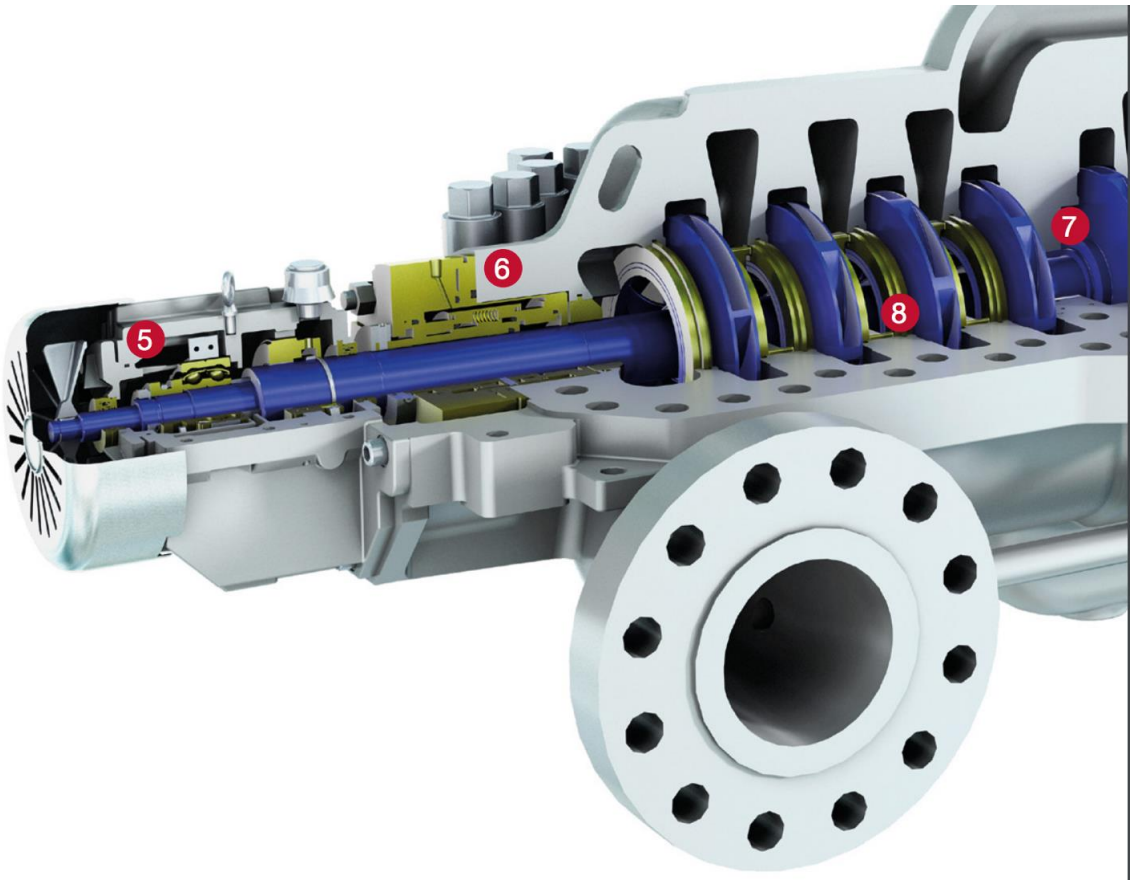

Figure 3: Schematic cutaway of pump similar to those in nuclear reactor systems. [7]

The RCIC pump takes its suction from one of two places: the Condensate Storage Tank (CST) or the suppression pool. The primary suction source is from the CST, which has the lowest suction source to verify there is reserved volume of water. The suction will change to the suppression pool if the CST water level gets too low.

The RCIC pump then discharges to two locations as well. As previously stated, the two discharges go to the feedwater spargers and the discharge

valve. The feedwater spargers distribute flow within the RPV, providing coolant over the entire core rather than a specific fuel assemblies. The discharge valve then provides the coolant to the turbine auxiliaries. The 400 GPM is provided to the feedwater spargers and 25 GPM is distributed to the discharge valves.

2.3 Fukushima Daiichi Accident Event Timeline

Nuclear operating stations are required to be able to safely shutdown in case of the largest recorded natural phenomena in the region. The Fukushima Accident was caused by two of the largest natural disasters the region has ever seen. Firstly, an earthquake that initiated the reactor SCRAM. This earthquake in turn caused a tsunami that was approximately 14 meters tall to hit the Fukushima Nuclear site. While the Nuclear site was designed to safely shutdown the earthquake, the site was only designed to withstand a tsunami up to 6 meters tall.

The tsunami was so great in size that it caused the flooding of the operating site. This flooding caused the loss of power to many of the systems required safety-related features set in place for an earthquake of the magnitude seen nearby. The RCIC system is capable of operating without power, as it is credited with 8 hours of power loss operating capability. This is under the assumption that power is able to be restored to the site within 8 hours, which was not the case in the Fukushima accident. The RCIC system was able to operate for 70 hours without the necessary power. The reason for this incredible

increase in performance is all speculative up to this point. The RCIC system performance is worthy of investigation in Beyond Design Basis (BDB), as seen in the Fukushima accident.

The design features of the RCIC system will help to describe in more detail the RCIC system during the Fukushima Accident. After the reactor SCRAM in unit 2 due to the earthquake, the RCIC system was manually started three times [4]. Once the first two startups occurred, there was an occurrence of the RPV high water level trip (L8), which caused the shutdown of the RCIC system. The tsunami hit almost immediately after the third manual startup of the system. The loss of DC power, as previously discussed, results in the failure of instrumentation blocking capability of the RPV to overfill. With these instruments failing there was no L8 trip for the third manual startup of the RCIC system. The instrumentation controlling the Governor valve also failed with the introduction of water due to the tsunami. The failure of the governor valve instrumentation results in the Governor Valve being locked in a fully open state. With the governor valve is fully open the turbine was in one of two states: overspeed trip set point was never reached, or the overspeed trip set point was passed and the overspeed trip failed. Since data from the accident is limited, we cannot be certain of either case.

2.4 Project Motivation

The objective behind this project is to clarify RCIC pump performance under degraded conditions including various pump speeds and inlet water qualities. We aren't exactly sure why Unit 2 operated for 70 hours, but it could be theorized that the RCIC system ultimately failed due to decreased flow cause by pump degradation incited by two-phase introduction in the pump.

The current project is to model the RCIC pump behavior for extended performance with two-phase flow being introduced into the system. The motivation of this research is to find, in greater detail, the capabilities of the RCIC system. As seen in Unit 2, there is reason to believe that the RCIC system is capable of performing in the accident conditions where two-phase flow is introduced into the turbopump.

2.5 Problem Statement

The reason for failure of the RCIC system is still unknown. With Computational Multi-Fluid Dynamics (CMFD) being tested on the RCIC turbine, testing was also done on the pump that is directly coupled to the turbine. It is believed that this pump was performing with two-phase flow occurring, thus, reducing the efficiency of the pump. The CMFD results of this study will show how the RCIC pump would perform with changing variables throughout the duration of the Fukushima Accident.

It is known that any pump will operate at a lower efficiency with the introduction of two-phase flow, either from cavitation in the pump or being taken into the pump initially. We would like to quantify the exact degraded efficiency we can expect from the pump.

2.6 Importance of Research

This research is important due to the lack of CMFD models created to display the degradation of pump performance of a centrifugal, horizontal, multistage, closed impeller type pump, to the author's knowledge. This pump type is fairly specific to the nuclear industry and these types of tests/models are going to be proprietary or manufacturers property that they are unwilling to part with. With the high pressure the pump would normally operate under, the introduction of two-phase flow would be rare. A more robust knowledge of the RCIC system, and these pump specifically, would increase in a greater knowledge in plants that operate with these nuclear safety systems.

2.7 Desired Data

There are many gaps in the knowledge available from the RCIC system performance at the Fukushima Daiichi site. With an expanded knowledge of the system in its current state and the transients that occurred, better prediction of its operating time could be obtained. The data that would help to predict the operating time includes, but is not limited to:

- Efficiency of RCIC pump

- Extent of efficiency loss due to two-phase flow
- Effect of pressure, temperature, and void fraction on pump performance
- Verification of Damage
    - The machinery from Fukushima is still not accessible due to increased radioactivity levels following the accident.

3 LITERATURE SURVEY

Centrifugal pumps are frequently used pumps across multiple fields, including: oil and gas, and nuclear. The RCIC pump operates by having various numbers of impellers rotate around the shaft of the pump. The shaft of the pump runs axially through the center of the impeller. The impeller is fixed to the shaft as the shaft rotates, causing the impeller to rotate with it. The impeller has an eye on the front of it with the shaft going through the middle. The fluid enters the eye and hits the back face of the impeller. As the fluid hits the back of the impeller, the impeller blades are then rotated and add energy to the fluid. The energy imposed on the fluid forces the fluid out radially from the impeller. The fluid is then follows the path of the casing into the next eye of the following impeller. As the fluid flows through all impellers, it obtains hydraulic head stage by stage. Each stage imposes an equivalent amount of head to the fluid as the previous. The fluid, after passing through all of the stages of the impeller, will have enough pressure to overcome the required pressure by the plant.

As each plant's layout is different that requires the pumps characteristics to be varied to match the requirements needed at each plant. This means the number of blades in the impeller and the number of impellers will change from plant to plant. The RCIC pumps all have the same design though. What is known about the RCIC pump at Fukushima is that is a horizontal, axially split, centrifugal, multistage pump. A horizontal pump means that its suction and

discharge piping are on the side of the pump. This is different than most centrifugal pumps which have a vertical discharge. The axially-split just signifies that the pump casing is split axially (the principal joint is parallel to the shaft). The centrifugal describes the force that acts on the fluid as it is forced between stages. The multi-stage refers to the number of impellers inside of the casing that act on the fluid.

The largest variation from plant to plant is the number of impellers within the pump. This is due to a variety of things but mostly: change in altitude between the pump and the RPV. For example, a RPV that is at a higher altitude will require a higher pressure, or head, for the fluid to be delivered to it safely. Other variations in the pumps include the inlet pipe diameter, optimal flow rate, and optimal rotational speed.

As previously stated, there are many different variations of RCIC pumps employed throughout the world. They are all similar but vary depending on performance requirements needed at individual plants. The number of blades in the impellers and the number of impellers required are dependent on the pump manufacturer. For this study, a RCIC pump manual from a different nuclear plant that employs the RCIC system was used.

3.1 Pump Cavitation

Cavitation within a pump also can occur in the Net Positive Suction Head (NPSH) is less than what the pump requires. The NPSH required ($NPSH_r$) is the

minimum energy of the fluid at the inlet of the pump. The NPSH actual ($NPSH_a$) is the actual fluid energy at the inlet above the vapor pressure of the fluid. Cavitation at the pump impeller can occur when the $NPSH_a$ is less than $NPSH_r$.

Cavitation involves the formation and collapse of a vapor bubbles formed in the suction of the pump. Vapor bubbles form when the local pressure drops below the saturation pressure of the fluid at the local temperature. As the vapor bubbles move closer to the impeller, the pressure of the fluid increases. The pressure will eventually increase to a point where the vapor bubble will collapse. The collapse of the vapor bubble can cause damage to the pump impeller, excessive noise and vibration within the pump.

As the RCIC system continued to operate for an extended period of time the conditions that is was operating were continually changing. The process of removing decay heat as the enthalpy of the water increases will increase the probability of failure within the system. The energy that is absorbed into the water by the decay heat of the core continually increases the temperature of the water. The increased temperature of the water will induce vapor formation once the water begins to obtain a high enough heat flux from the reactor core. The cavitation of water is what degrades the performance of the pump.

The pump impeller will also be damaged under two-phase conditions as well. Figure 4 shows an image of a normal pump impeller. The cavitation will collapse as the impeller increases the pressure of the fluid. This collapse will slowly begin to cause micro fractures on the surface of the pump impeller.

Figure 5 shows the same pump impeller after 2 years of cavitation damage. This damage would degrade the performance of the pump by reducing the energy imparted to the fluid. Damage, like seen in Figure 5, takes continual exposure to the conditions for extended time periods. Since the pump is assumed to have no preexisting damage and the time frame under this study is days instead of years, the degradation due to cavitation is neglected.

Figure 4: Pump impeller with no cavitation damage. [8]

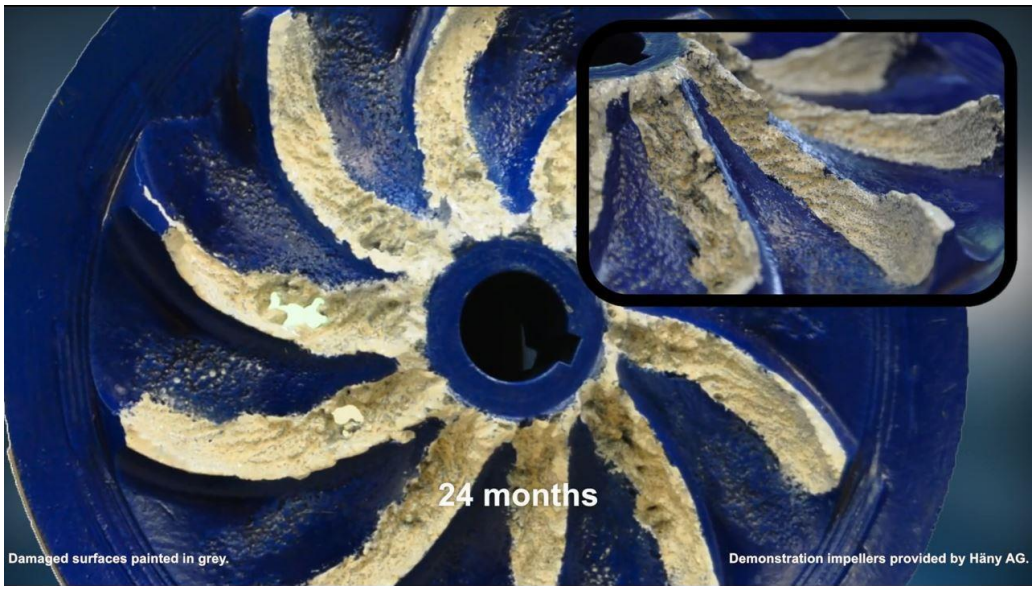

Figure 5: Pump impeller with damage from 24 months of cavitation damage. [8]

Modeled Pump Characteristics

Figure 6: An axially split centrifugal multi-stage pump similar to the one being modelled. [7]

In figure 6, the cutaway of a pump used in nuclear safety related systems around the globe is shown. This pump is similar to the one that will be modelled. The pump that will be modelled with have the following

- Optimal flow rate of 425 GPM
- Four stage impellers (Single Stage is used in CFD under assumption of equal head applied from each impeller)
- Variable Pump Speed from 2000 RPM- 3500 RPM

- Turbine Driven (Terry Turbine)
- Impeller diameter is 9 inches

The CAD model of a RCIC pump was created using the CAD modelling software SOLIDWORKS. The CAD model was created in likeness to the pump seen above in Figure 6. The exact specifications of the RCIC pump modelled cannot be detailed in this thesis due to the proprietary nature of the pump. The CAD Model of the impeller can be seen in Figure 7 below.

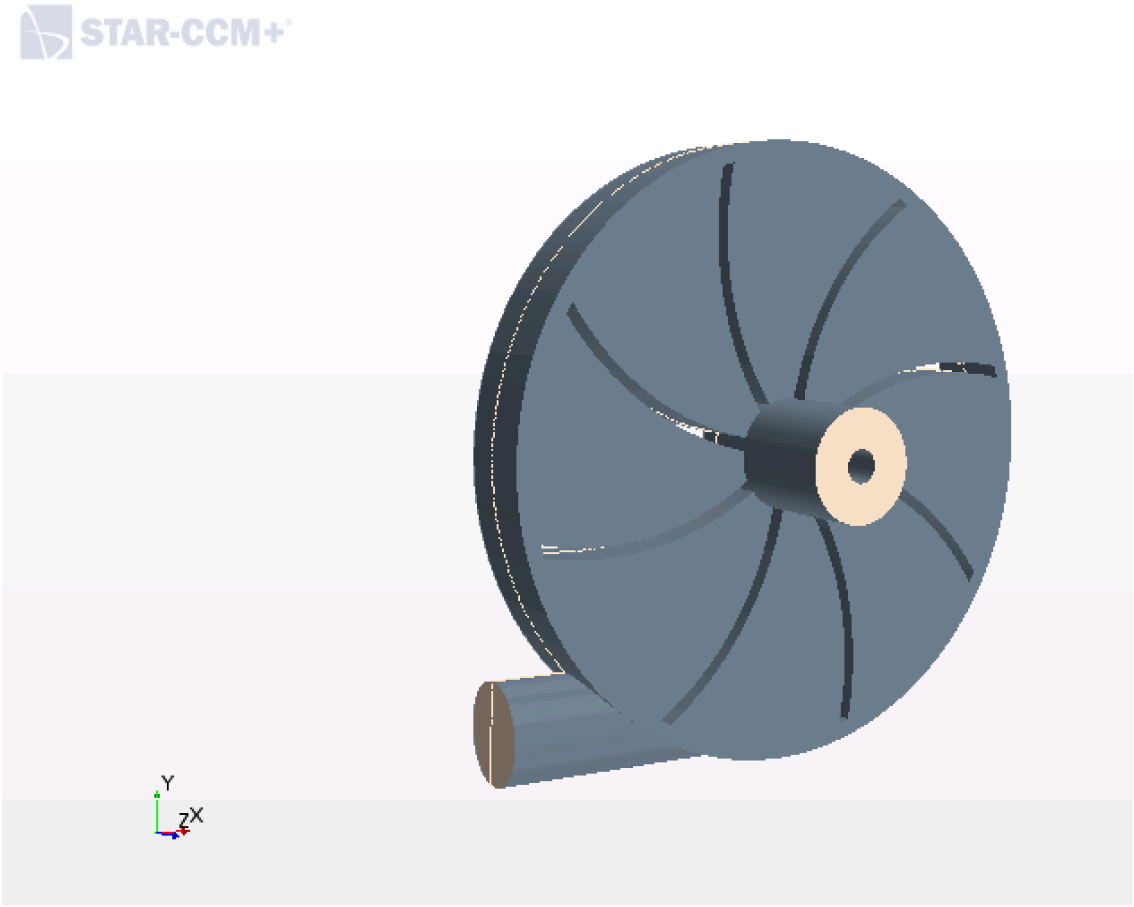

Figure 7: CAD model created for simulation of the RCIC pump.

The CAD model was created by creating a volume extraction from the pump casing and impellers. This provided a solid the area where fluid would actually be flowing. This allows STAR-CCM+ to mesh only the areas of interest to help decrease computation time. In Figure 7, seen above, the front of the model is the inlet while the side to the left is set as the outlet. There were two different regions specified in the model: the impeller and the casing. The casing was set to the regular reference frame while a special reference frame was created specifically for the impeller. The reference frame had to be created to capture the motion of the impeller. Within the reference frame, there is a setting for the user to dictate the direction and the rotational speed of the reference frame. Figure 8 depicts the reference frame that was set to rotate.

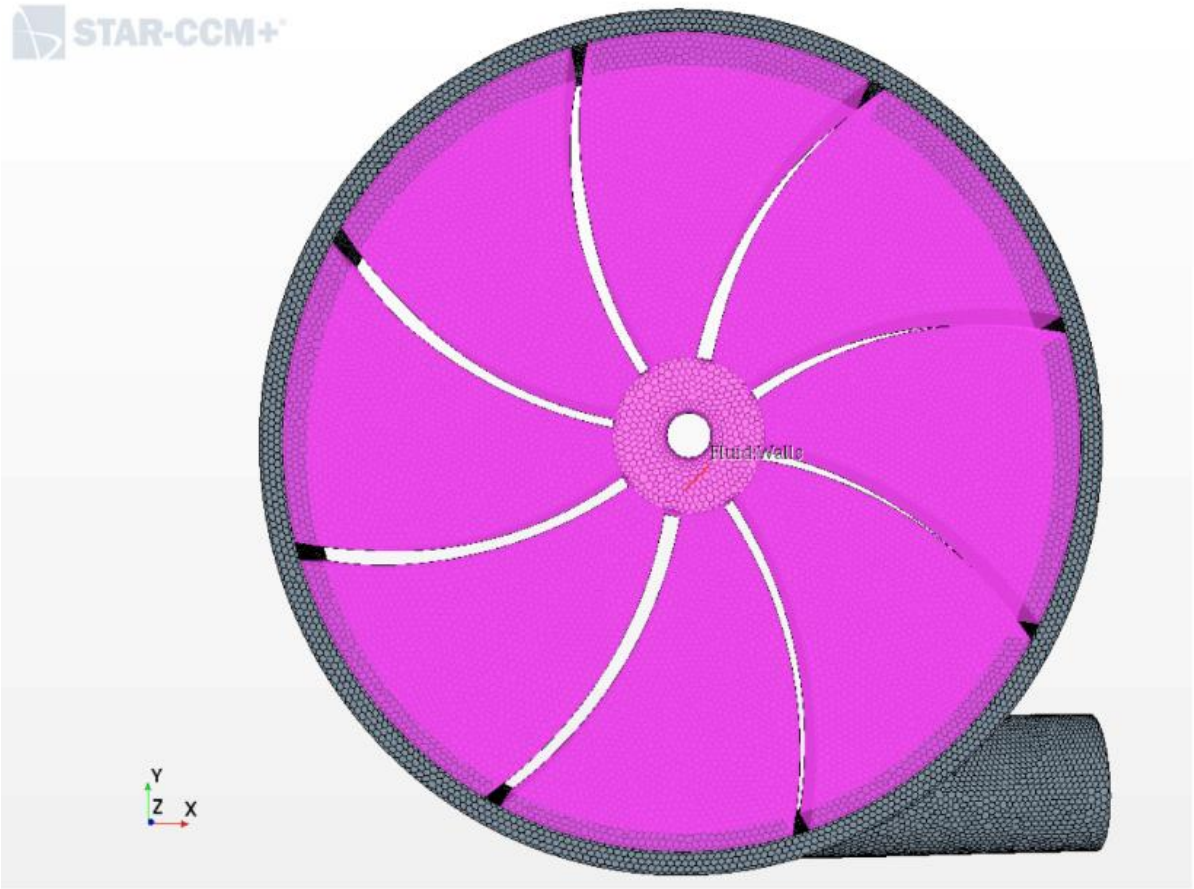

Figure 8: The rotation region that is set variable speeds in purple.

There were many specified boundary conditions input into the new model to help with computation. The two most important boundary conditions are set to the inlet and outlet. The inlet boundary condition was set as a mass flow rate inlet boundary condition to help stability of the simulation. The flow rate was specified as being perpendicular to the inlet face, meaning the flow was entering into the impeller. The outlet was set as a pressure outlet boundary condition. The boundary conditions for all of the walls were set as no slip walls. There was

also an interface boundary condition set between the two regions to transfer information between them.

The mesh was created in STAR-CCM+ using the automated mesh capabilities of the program. The meshing selections that were made include: polyhedral mesh, surface remesher, automatic surface repair, and prism layer mesh. The polyhedral and prism layer mesh were used to create the volume mesh while the surface remesher and automatic surface repair were used to create the surface mesh. There was also an increased mesh in the blades and edges of the wall. The base size, or target size for each cell, for the automated mesh was set to 0.02m. The number of prism layers was set to 12. The total prism layer thickness was set to 10% of the base. The high number of prism layers was used because of the turbulent nature of fluid in the pump, especially near the wall. This allows for greater accuracy of the solver in the near-wall region because of the no slip boundary condition set. Two figures below (Figure 9 and 10) are images of the mesh created in STAR-CCM+. The total number of nodes created in the mesh exceeded 22 million cells for both the casing and impeller combined.

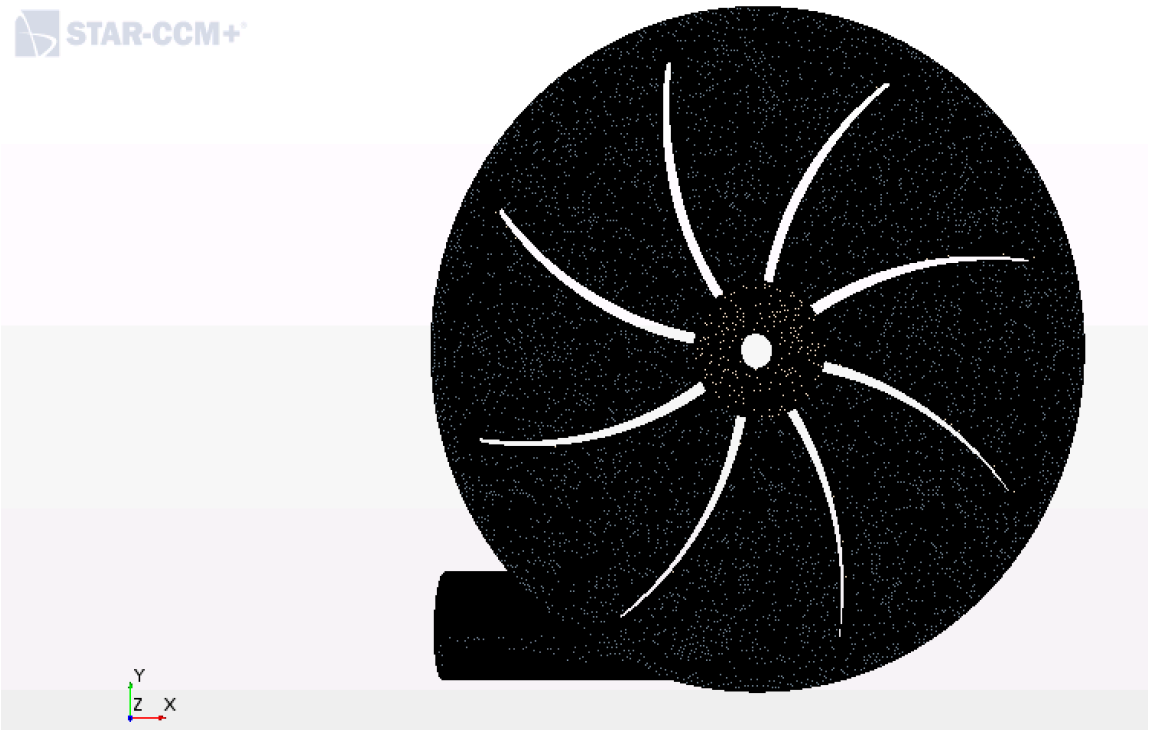

Figure 9: Front view of CAD model with mesh apparent.

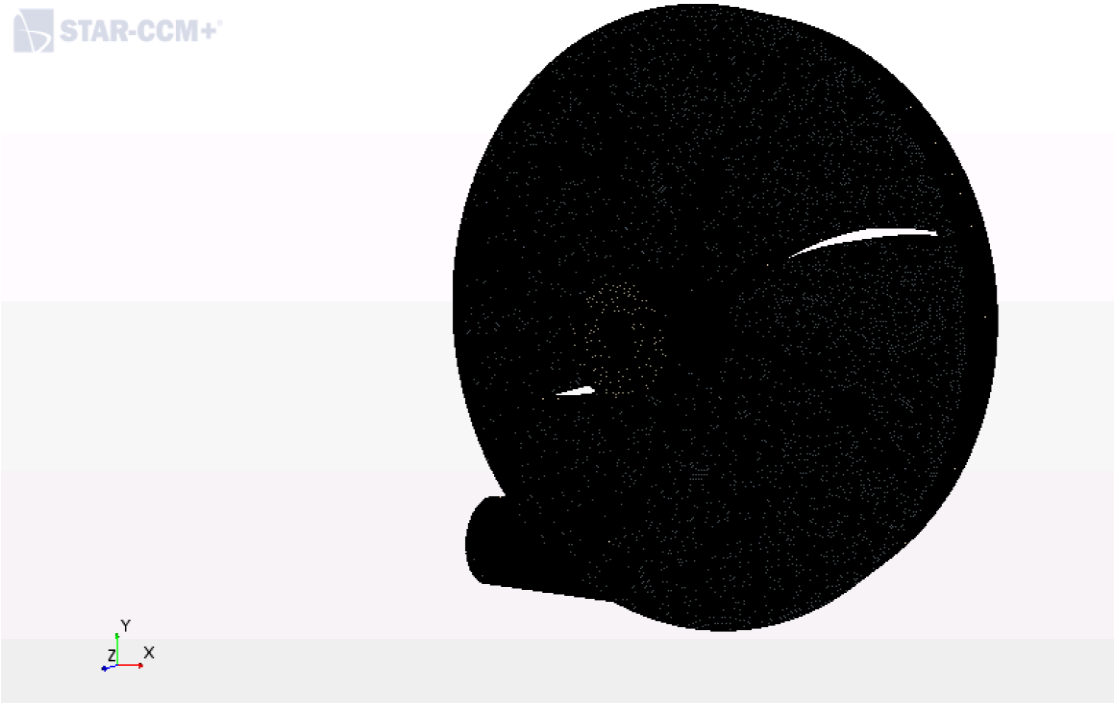

Figure 10: Side view of the mesh opposite of outlet.

4 PROGRAM BACKGROUND

STAR-CCM+ is a computer code that is now owned, maintained and operated by Siemens. It is capable of many different engineering applications, including:

- 3D CAD modeler
- Surface preparation functions
- Automated meshing technology
- Physics modeling
- Post-processing tools

The only application that wasn't actively used in the construction of this thesis was the 3D CAD modeler.

The 3D CAD modeler that was created using SOLIDWORKS. The SOLIDWORKS file was then imported into STAR-CCM+ and surface preparation was completed. Surface preparation is the process of readying the surface of the CAD model for meshing. This includes verifying that the surface is completely enclosed, and there are no pierced faces. The physics models that were selected for these simulations were taken as is from STAR-CCM+ physics models library. The Physics Models that were selected for the RCIC Pump include:

- Coupled flow and Coupled Energy model
- Eulerian Multiphase & Eulerian Multiphase Mixture

- Exact Wall Distance
- Gradients
- Multiphase Equation of State
- K-Epsilon Turbulence
- Multiphase Interaction
- Realizable K-Epsilon Two-Layer
- Reynolds-Averaged Navier-Stokes (RANS)
- Three Dimensional
- Two-Layer All y+ Wall Treatment
- Two-Phase Thermodynamic Equilibrium
- Steady-State time solver
- Turbulence Model

This computer code was selected to maintain unity throughout the project. The CFD that was performed on the terry turbine coupled directly with the pump was modelled using STAR-CCM+. This computer code was also accessible using a student license provided by Texas A&M.

Some of the common concepts used in STAR-CCM+ and in this thesis are described in detail in the subsequent paragraphs. The concepts include: simulations, parts, continua, models, regions, boundaries, interfaces, solvers, reports, monitors, plots, and scenes.

A simulation is the file that holds all of the data in regards to: physics models, mesh, and solution. The simulation is controlled through a graphic user interphase (GUI). In STAR-CCM+ there is an object tree set on the left side of the screen in which the user controls all aspects of the simulation.

Parts are components of the simulation that define its attributes. These can be multiple different things: geometry parts (imported CAD model), model parts, or derived parts. Geometry parts are viewed in the Geometry subsection in the object tree. Geometry parts can be edited using operations such as combining. Model parts are specific to regions, boundaries, and interfaces. These affect how the geometry is being analyzed. Derived parts are used more for extra analysis aspect: as visualizations and reports.

Models are the two different ways that the simulation can be changed: meshing and physics. Meshing models dictate the computation domain of the simulation. Regions are selected within the meshing models and then the meshing models are applied to those regions. Different meshing models include: Polyhedral, Tetrahedral, Surface Mesher, and Prism Layer Mesher. Physics models are how the user describes the problem that will be solved in the computational domain. The physics model and mesh model are often interdependent. For example, most turbulence models require a finer mesh at near wall locals (prism layer mesh). Another way these can be interdependent is specific locations of higher concern. In this simulation, the mesh was finer near the corner of the impeller blades.

Regions are volume domains that are completely enclosed using boundaries. Parts are assigned to regions which are then characterized by their meshing models. When information is needed to be transferred between two connecting regions an interface is used. This is used in my simulation between the impeller region and the volute casing region.

Boundaries are surfaces that completely envelop the region that it is assigned to. Boundaries are exclusive to the region it is assigned to meaning they cannot be shared by two different regions. A selection must be made in the object tree to dictate what type of boundary it is: mass flow inlet, wall, velocity inlet, stagnation inlet, pressure outlet.

When information is needed to be transferred between two boundaries that are assigned to different regions an interface is used. The information that is frequently transferred is the flow of mass, energy, momentum, and other properties defined by the physics continuum. An interface selection must be made in the object tree. This selection will dictate how the information is transferred across the interface.

Solvers are dictated by the selection of the physics models. They are activated a minimum of once per solution iteration, some cases more frequently for a greater convergence in the iteration. In the current simulations, an example of the solver is the coupled solver for the coupled flow physics selection. The solvers manage the procedure in obtaining a converged solution.

Reports, monitors, plots, and scenes are all ways of watching the simulation advance and analyzing the output of the simulation. Reports are used to calculate specific metrics from the simulation, for example, surface averaged pressure. Monitors are used to output specific quantities as the solution progresses. Plots are a visual way to display different data sets and the value as it progresses through the simulation. Scenes are a visual representation to depict a variety of quantities in the scene.

5 SIMULATION SETUP

5.1 Model Variations

Multiple parameters were varied to assess various aspects of the RCIC pump performance over a range of suppression pool accident conditions. The longer the postulated accident continues to progress, the higher the Suppression Pool saturation temperature can become due to RCIC turbine exhaust into the pool and the greater the probability is for steam to enter the RCIC pump suction. The increased saturation temperature could also cause vapor formation within the pump, further degrading the performance of the pump. In order to simulate the effects that pressure and temperature have on the RCIC pump, pump suction void fraction will be changed.

As with input conditions in the model, the volume fractions of gas and fluid are supplied by the code user. Within the simulation, the density and viscosity of the fluid and gas are required inputs. In order to calculate the density and viscosity of the fluid and gas, a Matlab script was written (in appendix) to calculate the density of water and steam at the saturation temperature of the operating pressure of the RCIC system. The volume fraction affects how the pump will perform as pressure and temperature change. Table 1 lists the differences in simulations completed during this study.

Rotational Speed (RPM)	Volume Fraction	Flow Rate (GPM)
2000	0.0	425
3000	0.0	425
3500	0.0	425
2000	0.1	425
3000	0.1	425
3500	0.1	425
2000	0.2	425
3000	0.2	425
3500	0.2	425
2000	0.3	425
3000	0.3	425
3500	0.3	425

Table 1: Test simulation conditions.

5.2 Physics Models

The flow in the pump is turbulent due to the high flow rate and the small eye inlet of the pump. The pump also imparts extra force to the pump causing greater amounts of turbulence within the pump. A detailed description of turbulence fundamentals can be found in [9].

STAR-CCM+ has eight different types of k-ε models available. The user must know what the optimal form of the model is applicable for the required application. In modelling, I selected the realizable two-layer k-ε model. This

was coupled with an all-y+ wall treatment. The specifics of these turbulence models will be found in the following paragraphs. The explanations in the following paragraphs are drawn from the STAR-CCM+ users guide [10].

The term “realizable” means that changes will be made to the standard k-ε model that align more correctly with empirical evidence from physics. Specifically, the way the dissipation equation is employed. One coefficient from the standard model is varied to be a function of mean flow. Realizable k-ε model was used to help produce results that would closer mimic that of empirical evidence. The purpose of this study is to examine real pump performance in accident conditions and the closer to physics the more applicable this study will be.

The term “two-layer” refers to the application of the k-ε model to the viscous sub-layer of the turbulent boundary layer. This turbulent boundary layer occurs at near wall locations. To do this a wall function approach is not needed because the dissipation and turbulent viscosity are dependent on the wall distance. The normal transport equation for turbulent kinetic energy (TKE) is solved, however. In the bulk flow cells (farther from wall) all the k-ε equations are solved. The two different layers (near-wall and bulk flow) are then blended. This model was selected due to the high Reynold’s number of the simulated flow. Wall function approach is needed for low Reynold’s number simulations and do not apply well to Reynold’s number simulations.

The term “all-y+” refers to the combination of low-y+ and high y+ wall treatment. The low-y+ signifies that the mesh is fine enough to resolve the near-wall viscous sublayer. The high-y+ signifies that the mesh is coarse and wall laws are used to represent near-wall regions. How the all-y+ treatment works is attempts to duplicate the low-y+ results when the mesh is fine enough and the high-y+ when the mesh is coarse. The all-y+ model provides a friction velocity near the wall and affects the TKE production term near the wall. The all-y+ model was selected as to reduce the mesh size required for the simulation. The blending approach helps to decrease the number of cells needed in the viscous sub-layer by combining the two solving techniques.

The turbulence kinetic energy transport equation is:

$$(5.1)\quad \frac{\partial}{\partial t}\int_V \rho_{avg} k dV + \oint_A \rho_{avg} k((\vec{u} - \vec{u}_{grid}) * d\vec{A}) = \oint_A \left(\mu_{avg} + \frac{\mu_t}{\sigma_k}\right)(\overrightarrow{\nabla k} * d\vec{A}) + \int_V \left(f_c G_k + G_b - \rho_{avg}((\epsilon - \epsilon_0) + Y_m) + S_k\right) dV$$

Where:

k = Turbulent kinetic energy [J/kg]; $\vec{u}_{grid}$ = Grid velocity [m/s]

μ_t = Turbulent viscosity [Pa*s] ; σ_k = Turbulent Prantl number

f_c = Curvature factor ; G_k = Production source term for k

G_b = Buoyancy production source term for k

ϵ = Turbulence dissipation rate [J/kg/s]

ϵ_0 = Ambient turbulence value ; Y_m = Dilation dissipation

S_k = Miscellaneous source term for k

The turbulence dissipation rate equation is:

$$(5.2)\quad \frac{\partial}{\partial t}\int_V \rho_{avg}\epsilon dV + \oint_A \rho_{avg}\epsilon((\vec{u}-\vec{u}_{grid})*\mathbf{d}\vec{A}) = \oint_A \left(\mu_{avg}+\frac{\mu_t}{\sigma_\epsilon}\right)(\overrightarrow{\nabla\epsilon}*d\vec{A}) + \int_V \left(f_c C_{\epsilon 1} S_\epsilon + \frac{\epsilon}{k}(C_{\epsilon 2}C_{\epsilon 3}G_b) - \left(\frac{\epsilon}{k+\sqrt{v_{avg}\epsilon}}\right)\left(C_{\epsilon 2}\rho_{avg}(\epsilon-\epsilon_0)\right) + S_\epsilon\right)dV$$

Where:

S_ϵ = Miscellaneous source term for ϵ ; $v_{avg} = \frac{\mu_{avg}}{\rho_{avg}}$

$\sigma_\epsilon, C_{\epsilon 1}, C_{\epsilon 2}, C_{\epsilon 3}$ are model coefficients

The closures that are need for the transport equations include: Turbulence production term, buoyancy production term, dilation dissipation term, and the turbulent viscosity term. The model coefficients closure must be specified as well. Turbulence is increased by interactions between the mean flow strain and turbulent stresses. The turbulence production term is representative of the rate that turbulence is introduced to the flow is defined by equation 5.3:

$$(5.3)\quad G_k = \mu_t S^2 - \frac{2}{3}\rho_{avg}k(\nabla*\vec{u}) - \frac{2}{3}\mu_t(\nabla*\vec{u})^2$$

Where:

$S = |\bar{\bar{S}}| = \sqrt{2\bar{\bar{S}}:\bar{\bar{S}}}$; $\bar{\bar{S}} = \frac{1}{2}(\nabla\vec{u} + \nabla\vec{u}^T)$, for S the strain rate tensor

The Buoyance production term is defined by equation 5.4

$$(5.4)\ G_k = \beta\frac{\mu_t}{\sigma_t}(\nabla T * \vec{g})$$

Where:

β = Thermal expansion coefficient

The dilation dissipation term defined in STAR-CCM+ is:

$$(5.5)\ Y_m = \frac{2k\epsilon}{c^2}$$

Where:

c is the speed of sound

The turbulent viscosity takes the following form:

$$(5.6)\ \mu_t = \rho_{avg} C_\mu \frac{k^2}{\epsilon}$$

Where:

$C_\mu = \frac{1}{A_0} + A_s U^{(*)}\frac{k}{\epsilon}$; $U^{(*)} = \sqrt{\bar{\bar{S}}:\bar{\bar{S}} + \bar{\bar{W}}:\bar{\bar{W}}}$; $\bar{\bar{W}} = \frac{1}{2}\left(\overline{\nabla\vec{u} + \nabla\vec{u}^T}\right)$

$\bar{\bar{W}}$ is the rotation rate tensor ; $A_0 = 4.0$; $A_s = \sqrt{6}\cos(\phi)$

$\phi = \frac{1}{3}\arccos\left(\sqrt{6}W\right)$; $W = \frac{S_{ij}S_{jk}S_{ki}}{\left(\sqrt{S_{ij}S_{ij}}\right)^3}$ and $S = |\bar{\bar{S}}|$

The turbulence kinetic energy equation is solved in all cells of the mesh in the two-layer approach. In the viscous sublayer, however, special treatments are used for the turbulent viscosity, turbulent dissipation, and turbulent kinetic energy production. The two-layer approach coupled with an all-y+ treatment blends the wall function (single equation) near-wall layer treatment with the two-equation treatment in the bulk flow. Blending is done on the turbulent dissipation rate and the turbulent kinetic energy production. The turbulent viscosity isn't blended due to its dependence on a length scale function. The length scale function takes the form seen in equation 5.7. Equation 5.8 depicts the turbulent viscosity ratio.

$$(5.7)\ l_\epsilon = f(y, Re_y)$$

$$(5.8)\ \frac{\mu_t}{\mu_{avg}} = f(Re_y)$$

There are different ways to treat the length scale function and the turbulent viscosity ratio, however, all treatments are written as a function of the wall-distance (y) Reynolds number, seen in equation 5.9.

$$(5.9)\ Re_y = \frac{\sqrt{k}y}{v_{avg}}$$

All of the correlations use the same dissipation seen in equation 5.10.

$$(5.10)\ \epsilon = \frac{k^{3/2}}{l_\epsilon}$$

For all equations using the length scale function and the turbulent viscosity ratio, the layer blending is dependent on a wall proximity indicator defined as:

$$(5.11)\ \lambda = \frac{1}{2}\left[1 + \tanh\left(\frac{Re_y - Re_y^*}{A}\right)\right]$$

Where:

$Re_y^* = 60$; $A = \frac{|\Delta Re_y|}{\text{atanh } 0.98}$; $\Delta Re_y = 10$

Such that the blended turbulent viscosity is defined as:

$$(5.12)\ \mu_t = \lambda \mu_{t_{k-\epsilon}} + (1-\lambda)\mu\left(\frac{\mu_t}{\mu}\right)_{2-layer}$$

Where:

$$\mu_{t_{k-\epsilon}} = Realizable\ k-\epsilon\ turbulent\ viscosity$$

6 UNCERTAINTY QUANTIFICATION

A grid independence study was performed to investigate the impact of the variation in the base size, or number of cells in the mesh. Two different sized meshes with variations in the total number of cells were created to see if a finer mesh would vary the results of the model. The total number of nodes in the primary mesh contained 23 million cells while the refined mesh contained 28 million cells. Figures 11 and 12 depict the comparison of the original mesh and the refined mesh. The mesh was refined uniformly throughout the model.

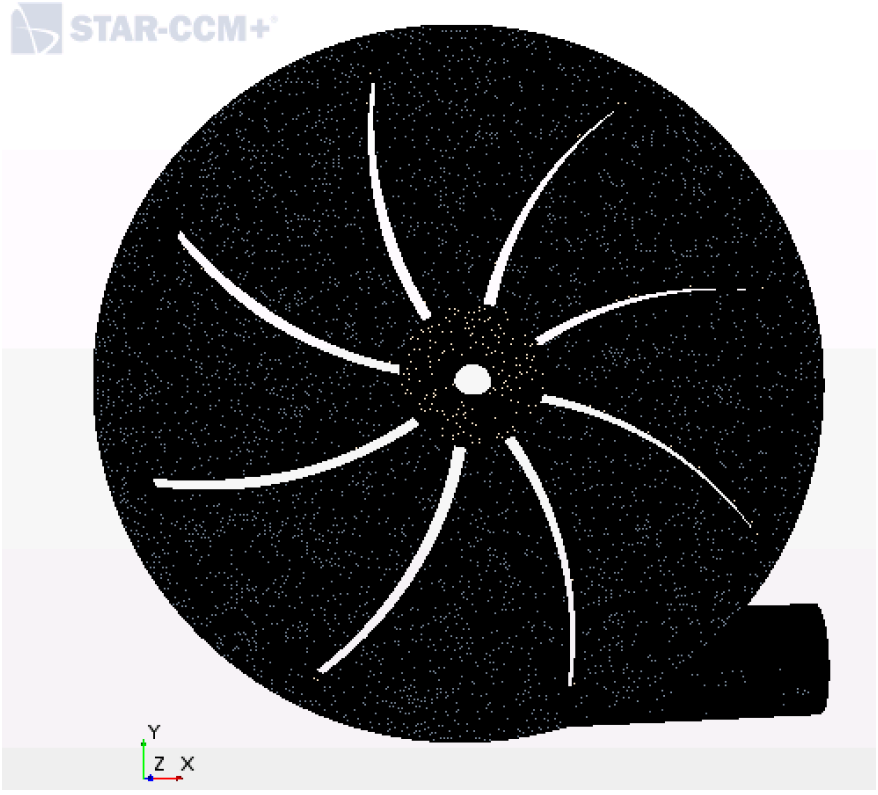

Figure 11: The original mesh used through the duration of the simulation.

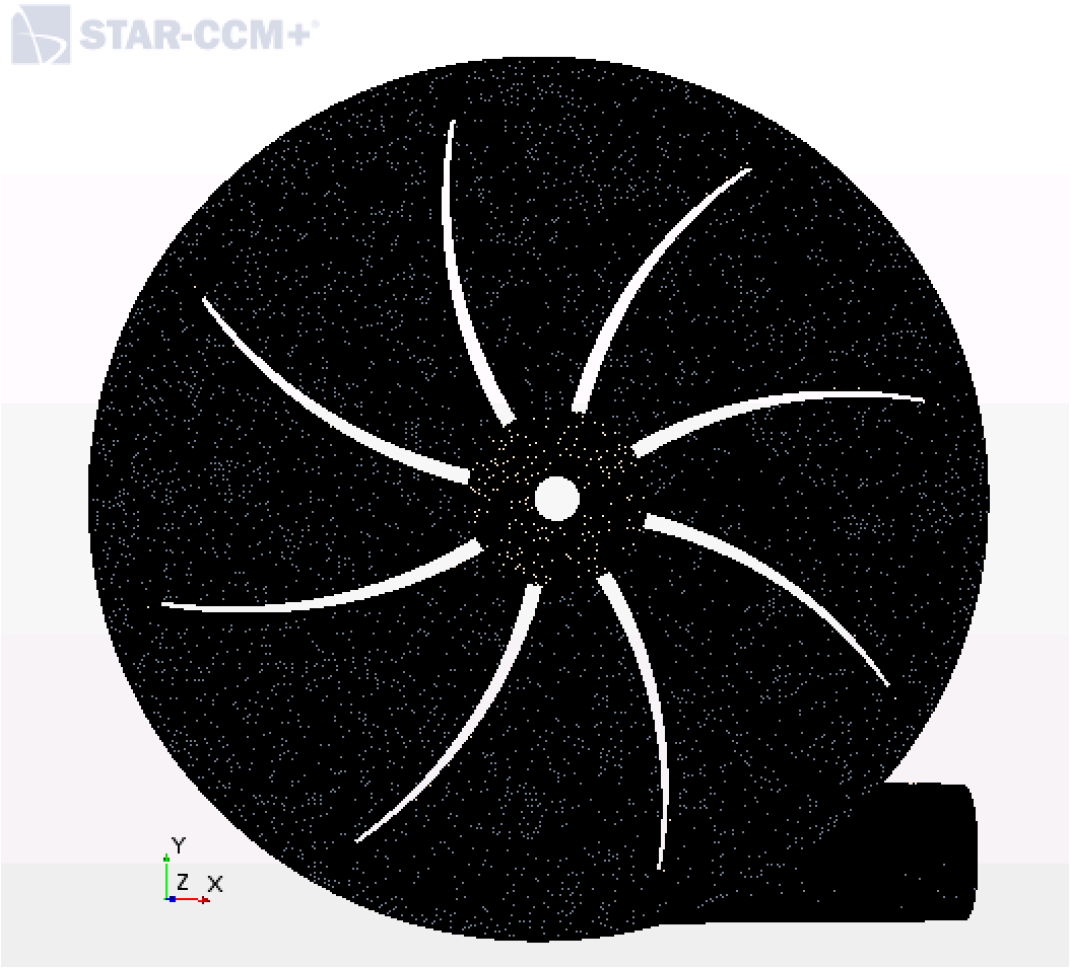

Figure 12: The refined mesh used to verify the grid independence.

In Table 2 the results of both models can be seen. In the final results, the pressure rise between the two stages is very similar. The pressure rise of the single stage changes merely 0.06%. This study verifies that changing the size of the mesh makes the change in simulation results negligible. This proves that the original grid is independent of the number of cells. The original grid was used for the remaining CFD simulations.

	Original Mesh	Refined Mesh
Cells	22907590	28400285
Pressure rise (Pa)	1137562	1144387
Ft. Head	1522.297142	1531.430925

Table 2: Comparison of the Grid independence study results.

7 RESULTS

The most important performance quality of a pump is the pressure rise, or the hydraulic head. In this study, the pressure at the outlet was set to a reference value of 1000 PSI in all cases. The pressure difference was recorded using a pressure drop function in STAR-CCM+. This function works by subtracting the higher pressure user selection from the lower pressure user selection. In the model the high pressure input is selected as the outlet. While the low pressure output is set as the inlet. The pressure drop uses a surface area average of the pressure of the entire outlet and inlet. Figure 13 depicts the location of the inlet pressure and the outlet pressure in the model.

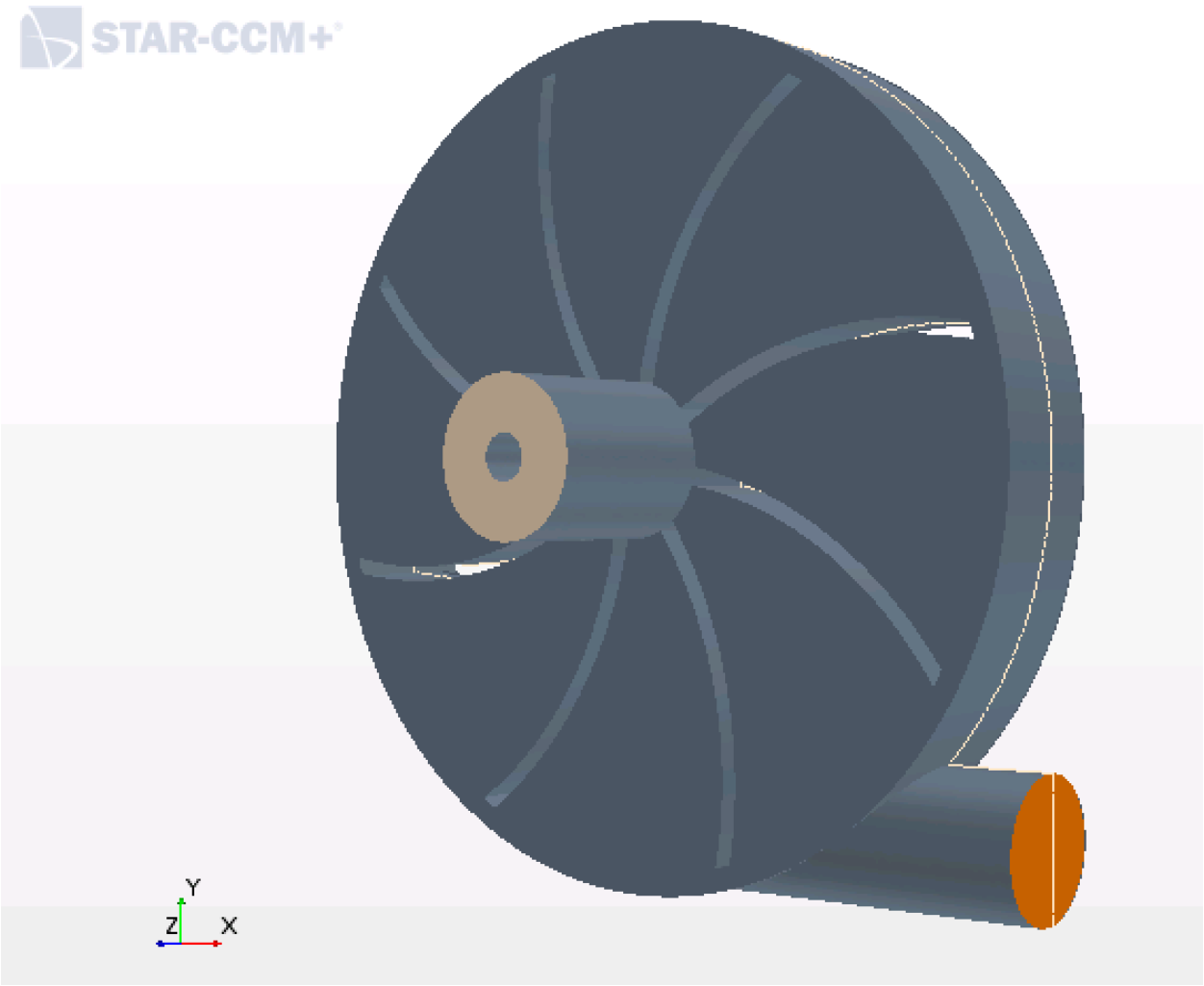

Figure 13: The position of the inlet pressure (tan) and outlet (orange) pressure in the model.

Figure 14 depicts the 2-D pressure contour at the outlet. Figure 15 is the pressure contour at the inlet. In figure 14 since the pressure at the outlet was set to be constant the pressure contour is also constant. In figure 15 is different at various points, the benefit of the area-averaged pressure of the pressure drop feature is beneficial.

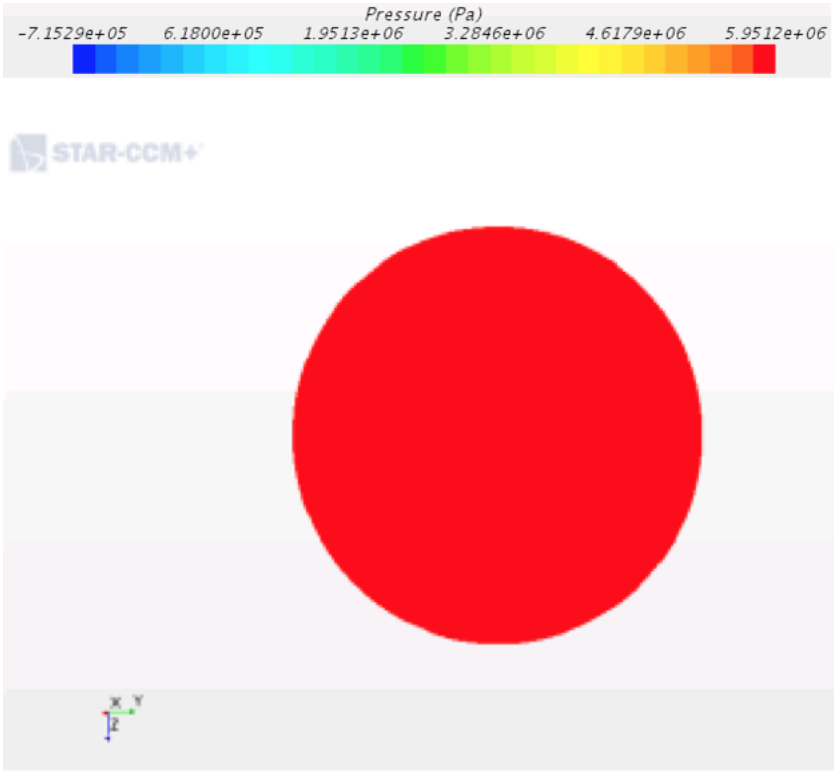

Figure 14: Outlet pressure from one of the simulations.

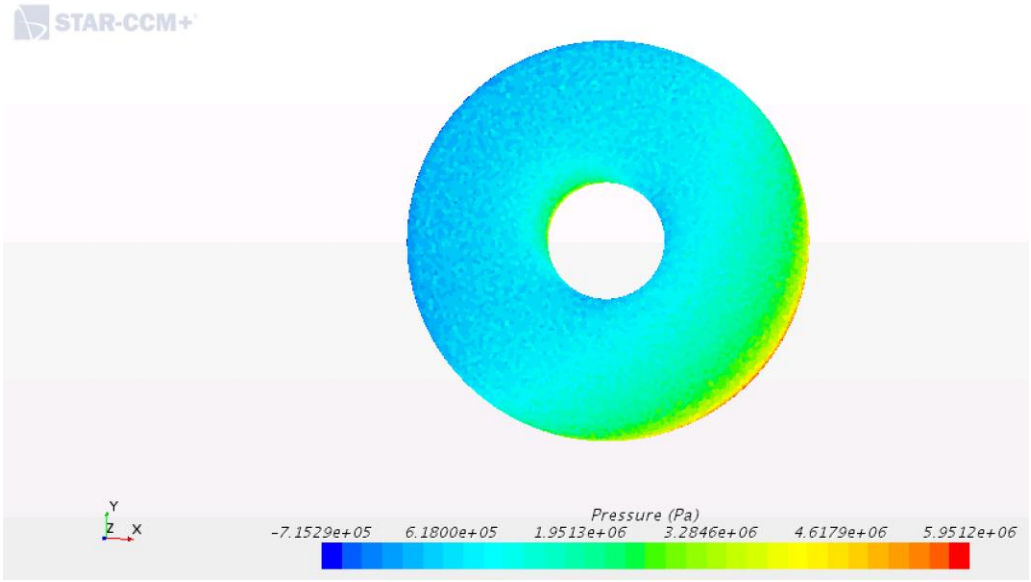

Figure 15: Inlet Pressure from the same simulation seen in figure 9.

The pressure rise of the whole stage is calculated as the negative of the pressure drop. This means the lower pressure inlet is subtracted from the higher pressure outlet.

In order to achieve the convergence the simulation was run for 600 iterations. This brought the TKE residuals down to the order of 10^{-2}. The residuals were continuing to decrease but at a rate so slowly that the simulation would have become to computationally expensive. The Wall-Y+, seen in figure 16, was also used to verify the mesh was refined to a sufficient point.

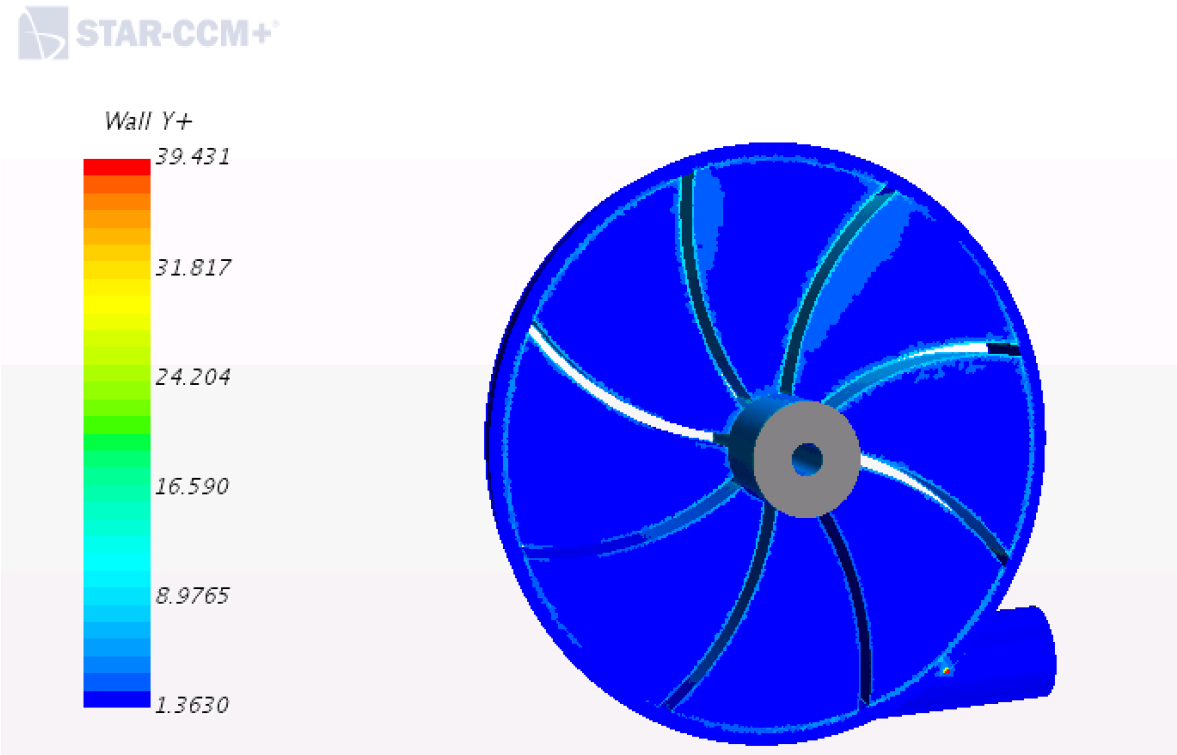

Figure 16: The Wall-Y+ was used to quantify the refinement of the mesh.

7.1 Performance Analysis

In order to study how the pump model performs in two-phase condition, an initial pump curve was created for normal operating condition. The pump curve is not as most normal pump curves look (Ft. head vs. Flow Rate) due to the constant flow rate required of the RCIC pump. This means that the variable examined within the model was the variable speed caused by the variable speed of the Terry Turbine. Figure 17 shows the pump curve used as a reference to dictate the effect of two-phase flow induction within the pump. Table 3 shows the results of the simulations to help comparisons as the large y-axis makes comparisons of small changes more difficult.

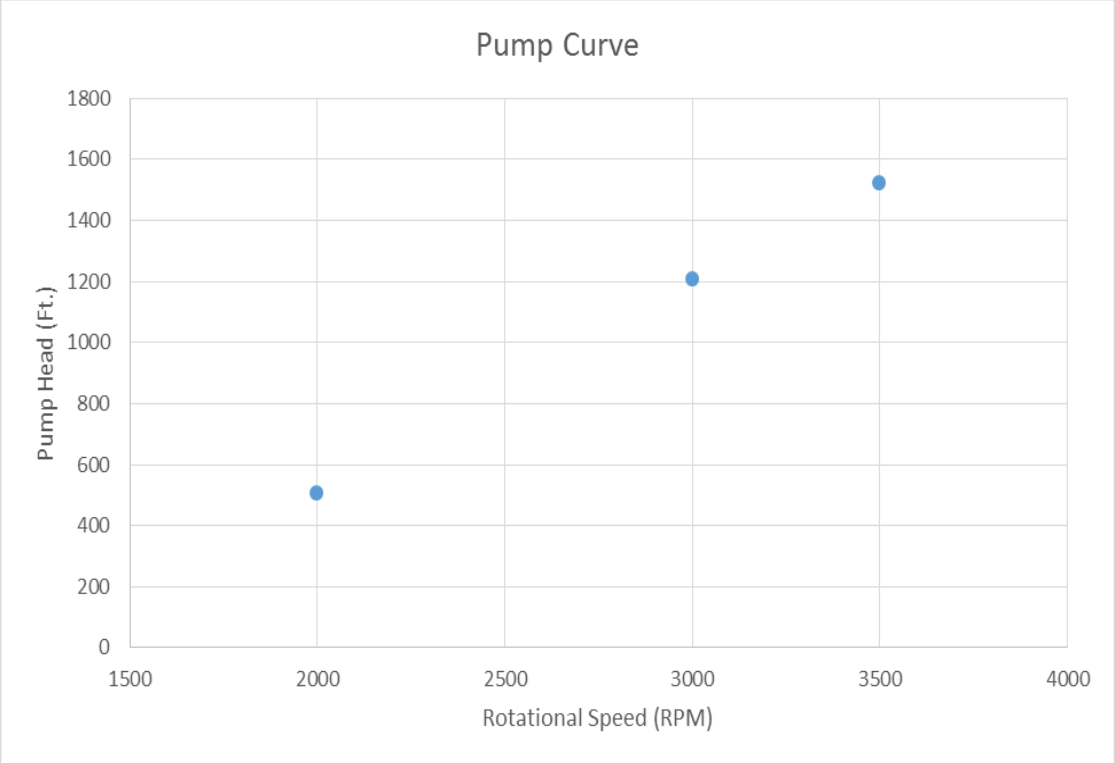

Figure 17: Pump model curve for performance as a function of rotational speed.

RPM	DP	Ft Head
2000	378318	506.27
3000	902656	1207.94
3500	1137562	1522.30

Table 3: The output results from the model simulations for the conditions of 100% water.

The pump curve seen, displays that the head of the pump increases as the rotational speed increases. This pump curve, initially, looks like a linear increase but if it is closely examined the curve takes more of a power curve. This type of curve means that a greater amount of head is caused by lower variations in rotational speeds at the higher rotational speeds.

Once the standard curve was created and verified to be what was expected out of the model the introduction of two-phase flow was the next step. The first simulation tested was for a pump that had a volume fraction 90% water and 10% steam throughout the entirety of the pump. The pump curve for the simulations containing those conditions can be seen in Figure 18. The exact output of the simulations can also be seen in table 4.

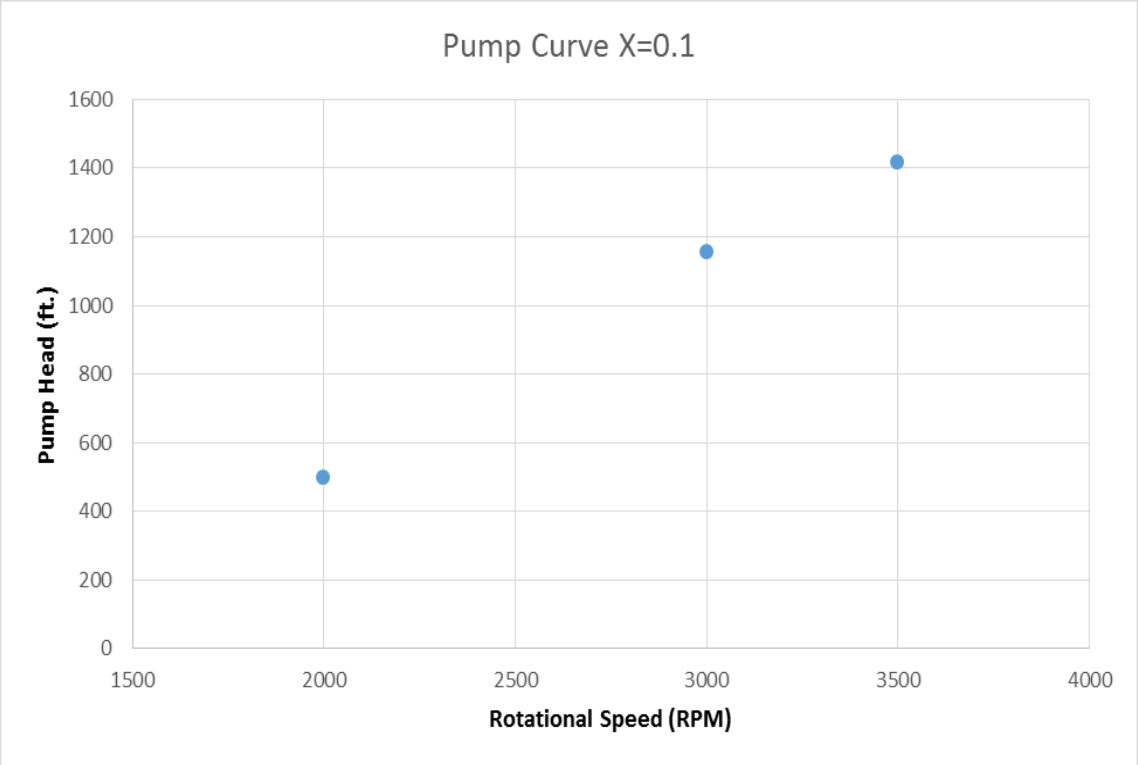

Figure 18: The pump curve for the model operating with 90% water and 10% steam at variable speeds.

RPM	DP	Ft Head
2000	373128.6	499.32
3000	862463.7	1154.16
3500	1058212.9	1416.11

Table 4: The output results from the model simulations for the conditions of 90% water and 10% steam.

The differences between Figure 17 and Figure 18 are difficult to see, however, the two tables make the differences more clear. The 2000 RPM simulations don't have a great amount of change as they are only ≈7 feet of head difference. The larger the rotational speeds, however, show a larger

change in the pump head difference. The largest difference in head is seen at the rated speed of 3500 being 106 feet of head.

The next set of simulations conducted was done with an even greater amount of volume fraction of steam. The set of simulations with the model was operating with a volume fraction 80% water and 20% steam within the pump. The pump curve for these simulations can be seen in Figure 119. The output results of the simulation can be seen in table 5.

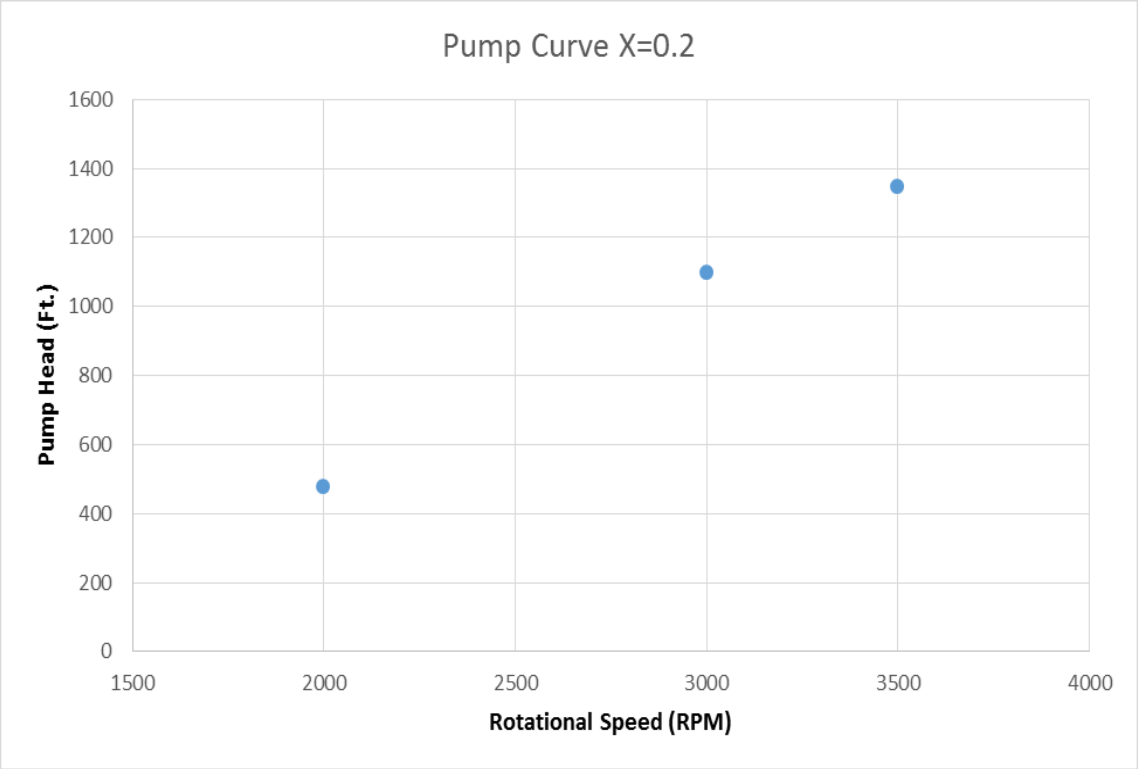

Figure 19: The output results from the model simulations for the conditions of 80% water and 20% steam.

RPM	DP	Ft Head
2000	355594.8	475.86
3000	820628.6	1098.17
3500	1005490.6	1345.56

Table 5: The output results from the model simulations for the conditions of 80% water and 20% steam.

The simulations with volume fractions of 80% water and 20% steam reflect similar results to that of the simulations with 90% water and 10% steam. The differences are within the degradation quantities as the 2000 RPM speed was degraded the least, with approximately 26 feet of head removed over the entire pump. The 3500 RPM simulation saw almost 200 feet of head removed in comparison to the normal operating conditions of the pump. This shows that the trend of the lower RPM simulations saw less degradation of head than that of the higher RPM simulations.

The next set of simulations saw a similar change as the previous, increasing the volume fraction another 10%. These simulations had 70% water and 30% steam volume fraction throughout the pump. The pump curve of the simulations can be seen in Figure 20. The results of the output of these simulations are contained in table 6.

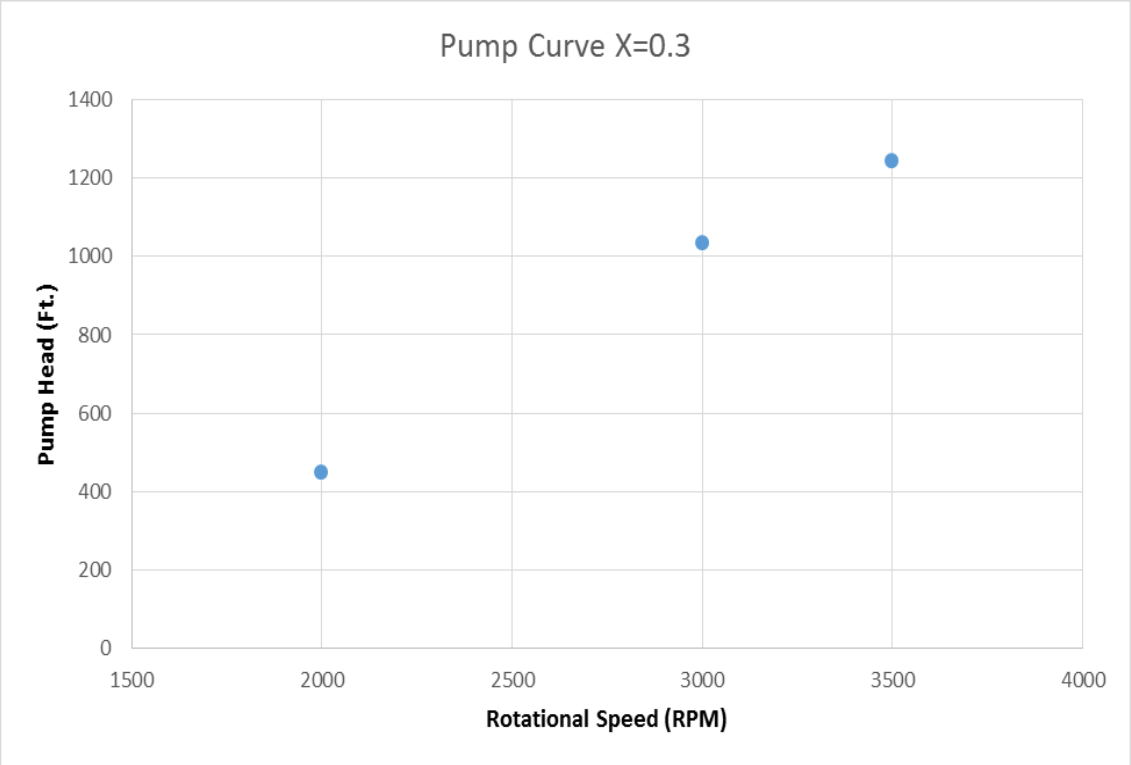

Figure 20: The pump curve for the model with the simulations being run with volume fractions of 70% water and 30% steam.

RPM	DP	Ft. Head
2000	335296.7739	448.70
3000	772475.846	1033.74
3500	928853.94	1243.00

Table 6: The output results from the model simulations for the conditions of 70% water and 30% steam.

The results of the 70% water and 30% steam volume fraction tests display that the results follow that of the previous simulations. The greater RPM simulations display a greater degradation of head. This of course is skewed by the fact that the overall head produced by the pump is greater so one would

expect a greater decrease in head. Figure 21 shows all of the pump curves created in this Thesis overlaid into one chart.

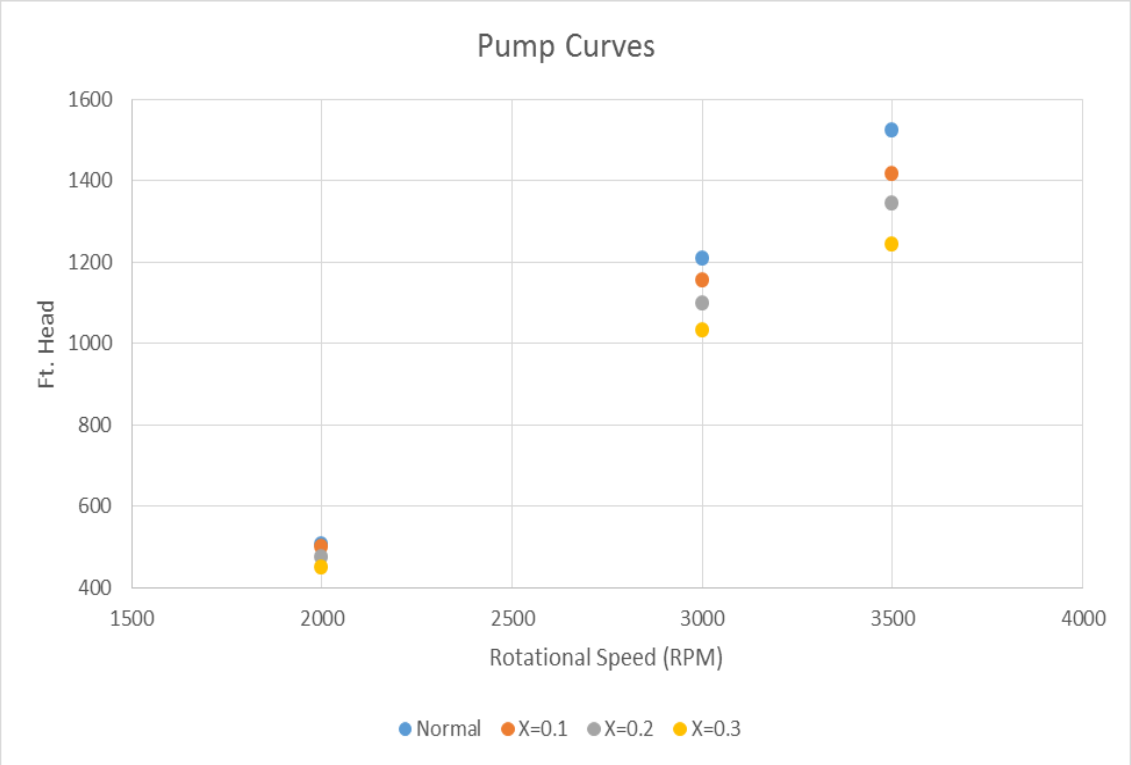

Figure 21: All of the previous pump curves displayed into a single figure for comparison.

The difference in pump performance is greatest at the highest rated speed of the pump model. The difference in performance is the least at the lowest rated speed of the pump. The increasing volume fraction causes increased divergence from each pump curve as the pump rotational speed increases. The 10% steam and 20% steam simulations acted similarly in pump head throughout. The 30% steam saw the greatest drop off from performance as one would expect.

7.2 Normalized Performance

As previously discussed, the results of degradation are skewed to the higher RPM simulations due to the increased head at those speeds. In an attempt to combat this a normalization of the head was used to display the results as a percent decrease. Equation 7.1 displays the way this normalized value was calculated. This allowed for a more direct comparison of how the pump performance was affected by the changing rotational speed. The pressure change was compared for the same rotational rate on the single phase flow to the two-phase flow. Figure 22 displays the normalized performance of the pump model under the volume fraction of 90% water and 10% steam.

$$(7.1)\ \varphi = \frac{DP_{TP\,flow}}{DP_{SP\,Flow}}$$

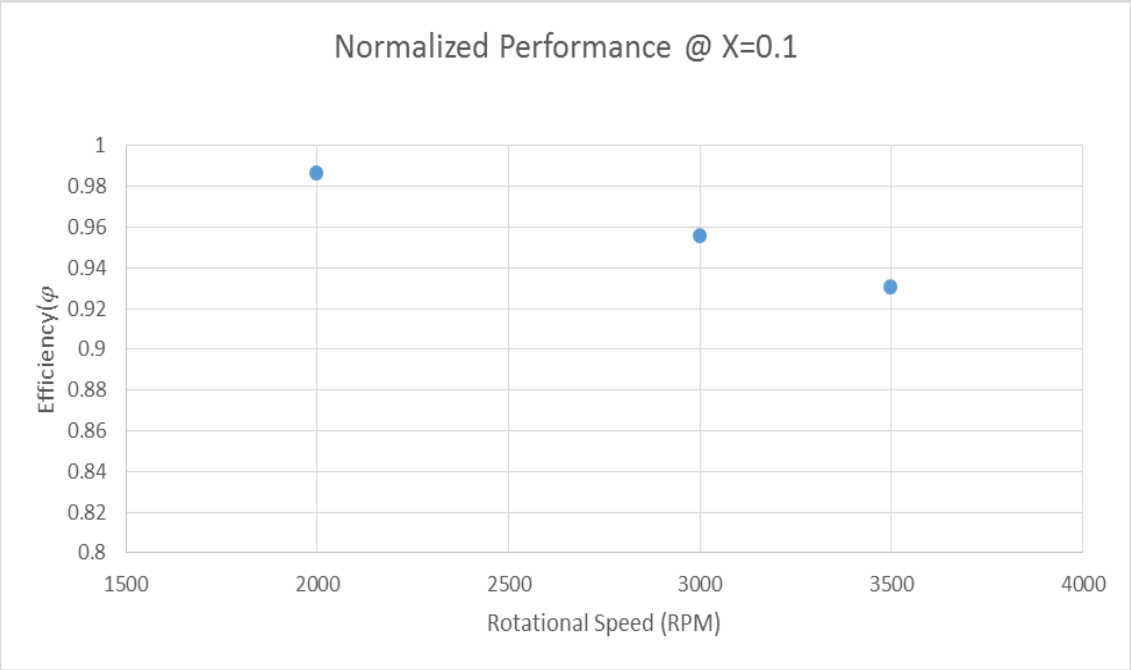

Figure 22: The normalized pressure increase of the pump under the volume fraction of 90% water and 10% steam.

The volume fraction of the steam can be seen as immediately impacting the performance of the pump, even at a low volume percentage. At the rated speed the two-phase flow degrades the pump performance by 7% of the optimal value in the model. The 3000 RPM head is degraded by just over 5%. This is the rated speed of the Z1 terry turbine used in Luthman [11]. The pump performance degrades just less than 2% at the lowest rated speed of the RCIC pump. This would dictate that should the terry turbine powering the pump fail prior to the failure of the pump the performance would not be greatly degraded at this volume fraction. The difference in performance at this volume fraction is approximately 6% between the lowest rated speed and the highest rated speed.

Equation 7.1 was also applied to the volume fraction split of 80% water and 20% steam. The pressure outputs of the simulation at this volume fraction split were compared to the normal performance of the pump model. The results of the equation application can be seen below in Figure 23.

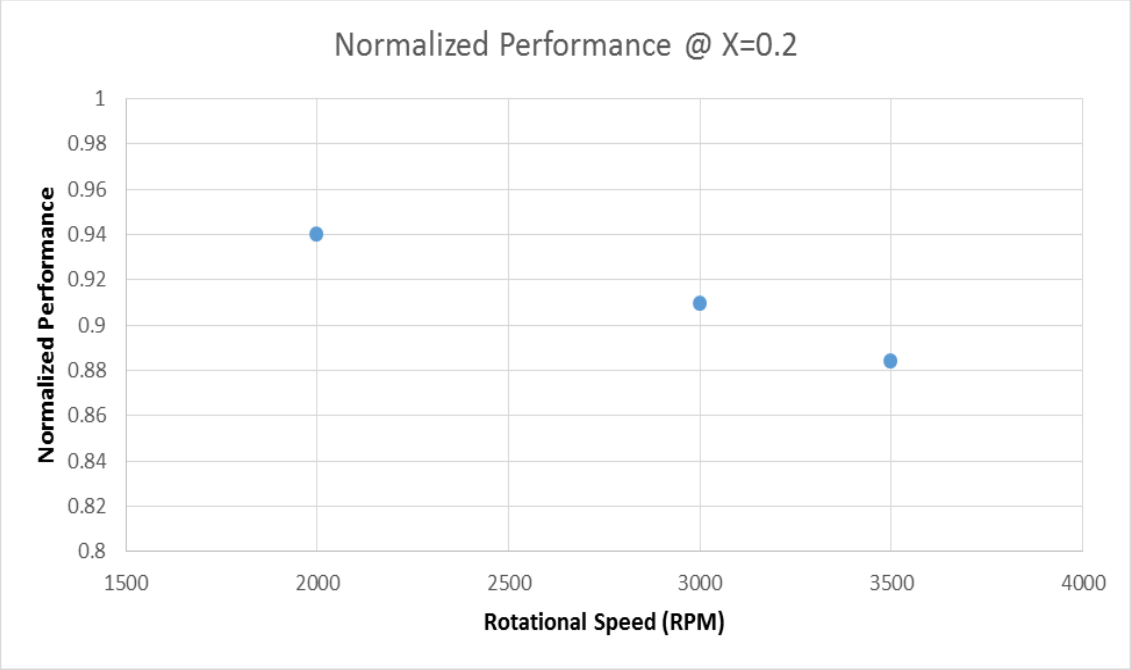

Figure 23: The normalized pressure increase of the pump under the volume fraction of 80% water and 20% steam.

Under the conditions of the 20% steam volume fraction, the pump model performance can be degraded over 10% of the rated head. The rated speed of the pump is degraded to almost 12%, with a small head, in relation to most nuclear industry pumps; this can immediately cause major issues. The lowest rated speed of the pump was comparable in percent degradation to the highest rated speed at the 10% volume fraction. The 3000 RPM value was also

degraded by approximately 9%. The difference in normalized pressure increase is similar to the drop in normalized pressure increase from 94% down to 88%.

Figure 24 shows the normalized performance equation (7.1) as a function of rotational speed with the volume fraction of 70% water and 30% steam.

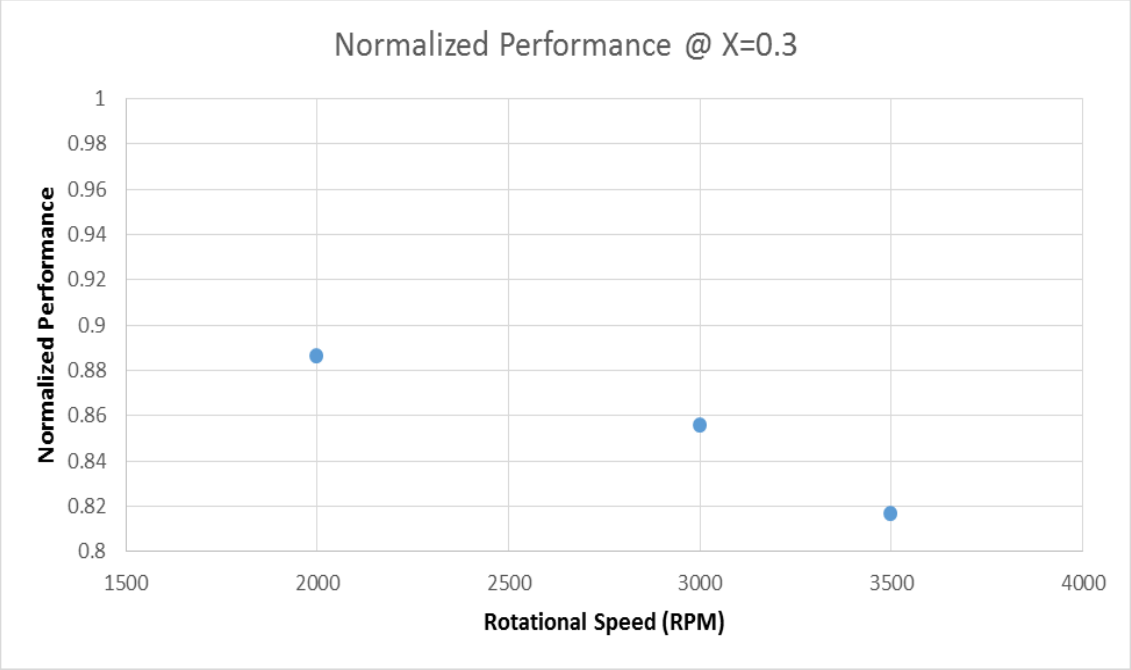

Figure 24: The normalized pressure increase of the pump under the volume fraction of 70% water and 30% steam.

The normalized pump performance at the the 30% steam is the lowest in relation to all of the other steam volume percentages. This follows the performance that would be expected; as the volume fraction of steam increases the performance of the pump will decrease. Similarly, to the comparison between the 10% steam and 20% steam the lowest rated speed has a similar performance to the highest rated speed at the 20% steam. The drop-in

normalized pressure increase is greater than that of other volume fractions. This is expected as the larger the volume fraction the greater decrease in performance. The optimal performance with the 30% volume fraction steam is 88% at the lowest rated speed of 2000 RPM. The most degraded performance occurs at approximately 82% at the maximum rated speed of 3500 RPM. The net difference in the maximum and minimum performance is 8%. This reduction is rather large for normal operating conditions of the pump. The variation in performance could have catastrophic results.

In an effort to better compare the normalized performance all three volume fractions were plotted together. The plot combining all three together can be seen in Figure 25.

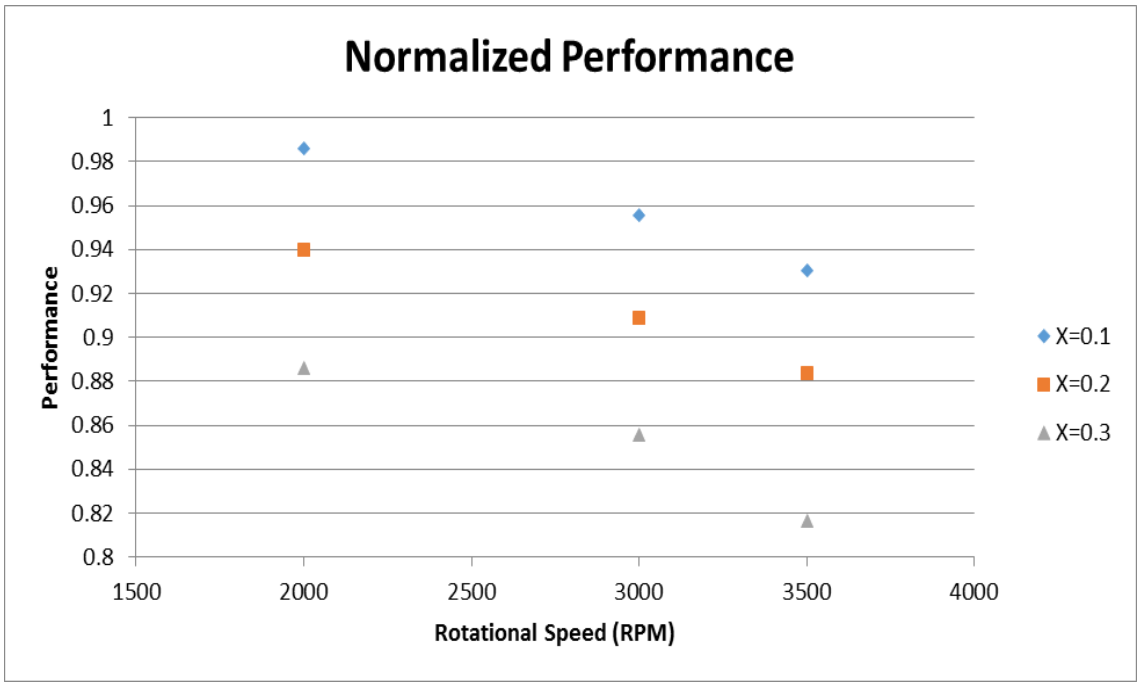

Figure 25: The normalized pressure increase of the pump under all volume fractions simulated with the pump model.

The first comparison to be made is the greatest drop off in pressure increase at the maximum rated rotation speed for the 30% steam volume fraction. This drop off proves that the larger the volume fraction the greater the pump degradation. The 10% steam has the smallest decrease in pump performance as the net difference in performance is only 6%. The 20% volume fraction steam has a 6.5% difference in performance. The decrease to almost 80% of performance could have catastrophic results. The reduced head could cause the pump head to be reduced to a point low enough that the flow cannot overcome the pressure difference between the pump and the feedwater spargers.

Equation 7.2 displays the definition of efficiency of pump performance.

$$(7.2)\ \eta = \frac{\rho_{avg} g Q H}{T \omega}$$

Where

ρ_{avg} is the average density; g is gravitational constant

Q is the flow rate (m^3/s) ; H is the pressure increase

T is the torque ; ω is the angular speed

While the pump performance will still decrease with varying rotational speed the study also needs to analyze how the pump efficiency will change with void fraction. Figure 26 displays the pump efficiency at the different rotational speeds of the pump. Only two set of data points were included due to the consistency in efficiency over the entire volume fraction models.

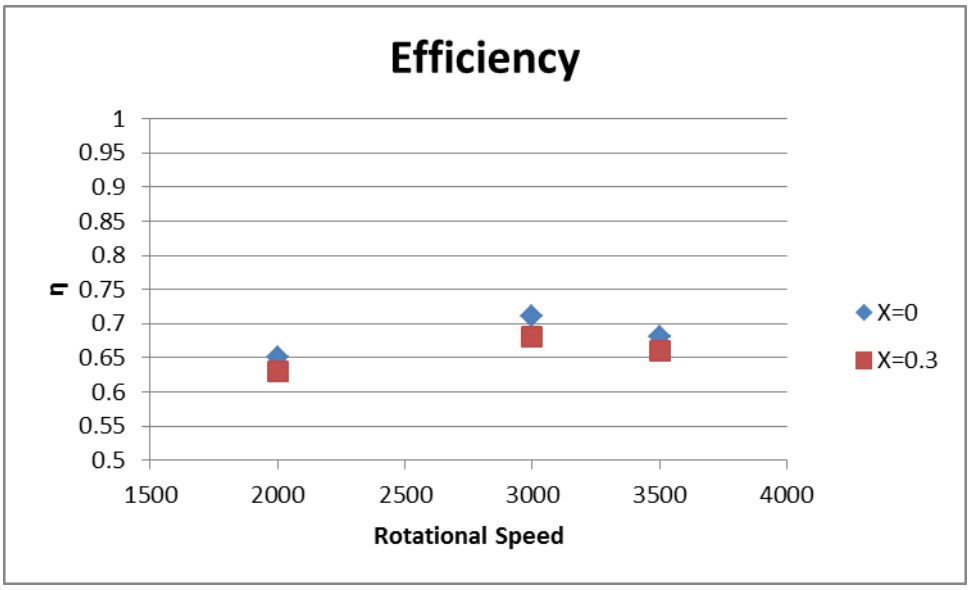

Figure 26: Efficiency curve for pump model created at normal operation.

Figure 26 displays that efficiency of the pump in my simulation wasn't varied greatly. This is due to the conservation of the pump affinity laws. The pump affinity laws dictates that efficiency will not appreciably change within the range of normal pump operational speeds. This can be seen as the efficiency doesn't change more than 3% at the maximum difference on the efficiency curve.

8 CONCLUSIONS

8.1 Commentary on Results

The results conclusively showed that the pump performance would be degraded with the introduction of two-phase flow at the inlet of the pump. At the normal operating condition of the pump model the performance can be degraded as much as low as 82%. The pump model can also be degraded as little as only 99% of its normal performance. We do see that as the volume fraction of the steam increases within the system the pump model head is it at its most degraded condition. The higher the volume fraction the greater the degradation will be at the optimum rotational speed of the pump. This indicates that if the pump was rotating at its intended speed during the Fukushima accident that the pump would have been operating at an even greater degradation value. However, since studies show the turbine performance was also degraded by the conditions of the accident [11], the pump would have been operating at a lower rotation speed. This would indicate that the degradation of the pump wouldn't have been as severe, even though it could have been operating below 90% its normal performance if the volume fraction of steam was great enough. The pump performance in the Fukushima Daiichi accident would be degraded, however, the amount of degradation is dependent on the amount of two-phase flow occurring within the pump.

8.2 Future Work

While this study did produce more insight into the works of the RCIC system during the operating conditions of the Fukushima Accident, greater amounts of information is needed. The first action would to be conduct greater uncertainty tests within my model, specifically the input uncertainty. Other work would be to include the collapsing bubbles and creation of bubbles within the impeller region of the pump. This includes the drop of pressure due to a system break or leak down to atmospheric pressure. A more comprehensive model of the pump should be created with greater detail to help model the formation and collapse of bubbles within the model. Work should also be done to study to effect of potential heat up of the pump casing, this could cause impeller lockup due to overheating of the oil. While there have been computer simulations conducted on the turbine [12] and experimental results to validate [11] experimentation for the pump has not been studied. The most important test possible would be experimental tests for validation of my CMFD model. If these test were completed that would create a more complete study of the pump operation within the accident conditions experienced at Fukushima.

REFERENCES

[1] General Electric, “General Electric Systems Technology Manual, Chapter 2.7, Reactor Core Isolation Cooling System” 2012.

[2] General Electric, “General Electric Systems Technology Manual, Chapter 6, BWR Differences” 2017.

[3] International Atomaic Energy Agency, “The Fukushima Daiichi Accident”, Technical Volume 2, Safety Assessment, IAEA, Vienna, Austria, 2015.

[4] R. Gauntt, D. Kalinich, J. Cardoni, J. Phillips, A. Goldmann, S. Pickering, M. Francis, K. Robb, L. Ott, D. Wang, C. Smith, S. St. Germain, D. Schweide and C. Phelan, “Fukushima Daiichi Accident Study (Status as of April 2012),” Sandia National Laboratories, Albuquerque, 2012.

[5] K. Ross, J. Cardoni, C. Wilson, C. Morrow, D. Osborn, and R. Gauntt, "Modeling of the Reactor Core Isolation Cooling Response to Beyond Design Basis Operations,” Sandia National Laboratories, Albuquerque, 2015.

[6] Y. Yamanak, S. Mizokami, M. Watanabe and T. Honda, “Update of the First TEPCO MAAP Accident Analysis of Units 1, 2, and 3 at Fukushima Daiichi Nuclear Power Station,” Nuclear Technology, 186(2), pp263-279, 2014

[7] Sulzer, “MSD/MSD2 Axially Split Multistage Pump Brochure,” Sulzer, 2014.

[8] WCNOC, “Gas Accumulation Training/ Gas Voiding Events Wolf Creek,” WCNOC, 2016

[9] CD ADAPCO, “STAR-CCM+ User Guide,” 2016.

[10] CD ADAPCO, “STAR-CCM+ Theory Guide,” CD ADAPCO, 2016.

[11] N. Luthman, “Evaluation of Impulse Turbine Performance Under Wet Stream Conditions,” Office of Graduate and Professional Studies of Texas A&M University, 2017.

[12] B. Beeny, “Computational Multiphase Fluid Dynamics Analyses and Systems-Level Model Development for a Reactor Core Isolation Cooling System Terry Turbine”, Office of Graduate and Professional Studies of Texas A&M University, 2017.

APPENDIX A

```
clear all
clc
P_iso = 34.4738; %800psia to bar
T_sat= XSteam('Tsat_p',P_iso);
T= T_sat+1;
rho_f = XSteam('rhoL_p',P_iso);
rho_g = XSteam('rhoV_p',P_iso);

%% Dynamic Viscosity Calculations
Viscosity = XSteam('my_Pt',P_iso, T);

%% Flow Rate Converisions
Flow = 425;%GPM
flow_factor = .003785*rho_f/60; %Gallon to m^3*Density of water
(kg*min/Gallon*s)
Flow_rate= Flow*flow_factor; %Kg/s
```